Effect of localized input on bump solutions in a two-population neural-field model

Muhammad Yousaf[a,b], John Wyller[a,*], Tom Tetzlaff[c], Gaute T. Einevoll[a]

[a] *Department of Mathematical Sciences and Technology, Norwegian University of Life Sciences, P.O. Box 5003, N-1432 Ås, Norway*
[b] *Department of Mathematics, COMSATS Institute of Information Technology, Lahore, Pakistan.*
[c] *Inst. of Neuroscience and Medicine (INM-6), Computational and Systems Neuroscience, Research Center Jülich, Germany.*

Abstract

We investigate a two-population Wilson-Cowan model extended with stationary and spatially dependent localized external inputs and study the existence and stability of localized stationary (bump) solutions. The generic situation for this model in the absence of external inputs corresponds to two bump pairs, one narrow and one broad pair. For spatially wide localized external inputs we find this generic picture to be unchanged. However, for strongly localized external inputs we find that three and even four bump pairs, all with symmetric activity profiles around the center of the localized external input, may coexist. We next investigate the stability of these bump pairs using two different techniques: a simplified phase-space reduction (Amari) technique and full stability analysis. Examples of models, i.e., choices of model parameters, exhibiting up to three stable bump pairs are found. The Amari technique is further found to be a poor predictor of stability in the case of strongly localized external inputs. The bump-pair states are also probed numerically using a fourth order Runge-Kutta method, and an excellent agreement is found between numerical simulations and the analytical predictions from full stability analysis.

Keywords: Two population neuronal-field models, Localized input, Bumps solutions(see below), Localized solution, Integro-differential equation,

*Corresponding Author: Tel. +47-64965489, Fax: +47-64965401
Email address: John.Wyller@umb.no (John Wyller)

Stability analysis, Fourth-order Runge-Kutta method.

1. Introduction

Experiments have implicated persistent neuronal firing a possible substrate for short-term memory [1, 2, 3], and this has spurred significant interest among modelers in investigating persistent neural-network activity [4, 5, 6, 7] and, in particular, spatially localized activity solutions, 'bumps', of neuron network models [7, 8]. In recurrent networks such localized stationary states are naturally formed by a combination of (i) a strong and localized recurrent excitation boosting the bump and (ii) a spatially more extended 'lateral' inhibition preventing the bump from growing in size [9]. Neuronal field models have provided a powerful and versatile tool for the investigation of the properties of such bump states [8, 9, 10, 11, 12, 13], and a large number of studies have used such models to study generic properties of bumps such as conditions for their existence and stability [14, 15, 16, 17, 18, 19, 20, 21, 22, 23, 24, 25, 26, 27].

Most of these studies have focused on the generic properties of bumps for spatially homogeneous, i.e., translationally invariant, networks without external inputs. In some studies homogeneous inputs has been included [9, 14, 20]. However, as such inputs do not violate the translational invariance of the model, few new qualitative features are introduced, and the effects are akin to changing the effective firing threshold in the neural-field firing-rate functions. A more interesting situation arises when the external input is spatially localized as this breaks the translational invariance. Further, the situation with such localized inputs is expected to be common in real neural networks, for example, in primary visual cortex where such inputs must underlie the prominent retinotopic organization [28]. Models with localized inputs have been explored in the context of orientation tuning in visual cortex [29, 30]. In a more general setting, Folias et al [19] analyzed bumps in a one-population model with spatially localized external inputs and found that (i) sufficiently large inputs can stabilize bump states and (ii) that reduction of the input amplitude may induce a Hopf instability and the conversion of stable bumps into breather-like oscillatory waves.

In the present study we investigate the effects of spatially localized external inputs on bump states in a two-population Wilson-Cowan like model with one excitatory and one inhibitory population. We have previously investigated bump states in this model without external inputs [24, 27], and an

interesting feature is the key role played by the inhibitory time constant in determining the stability of bumps. The bumps are found to be stable only for inhibitory time constants below a critical value, about three times the excitatory time constant for the example in [24], while the bumps are converted to stable breathers through a Hopf bifurcation at the critical value. This crucial dependence on the ratio of inhibitory and excitatory time constants, which obviously cannot be addressed in a one-population model, has previously been seen in extensive network simulation of integrate-and-fire neurons [4, 6].

The model investigated is a direct extension of the model studied in Blomquist et al [24] with spatially dependent external inputs added to the equations describing the dynamics of both the excitatory and inhibitory populations:

$$\begin{aligned}
\tfrac{\partial}{\partial t}u_e(x,t) &= -u_e(x,t) + \textstyle\int_{-\infty}^{\infty}\omega_{ee}(x'-x)P_e(u_e(x',t)-\theta_e)dx' \\
&\quad - \textstyle\int_{-\infty}^{\infty}\omega_{ie}(x'-x)P_i(u_i(x',t)-\theta_i)dx' + h_e(x) \\
\tau\tfrac{\partial}{\partial t}u_i(x,t) &= -u_i(x,t) + \textstyle\int_{-\infty}^{\infty}\omega_{ei}(x'-x)P_e(u_e(x',t)-\theta_e)dx' \\
&\quad - \textstyle\int_{-\infty}^{\infty}\omega_{ii}(x'-x)P_i(u_i(x',t)-\theta_i)dx' + h_i(x)
\end{aligned} \tag{1}$$

Here $u_e(x,t)$ and $u_i(x,t)$ are excitatory and inhibitory activity levels, $\omega_{mn}(x)$ the distance-dependent connectivity strengths, P_e and P_i the firing-rate functions for the excitatory and inhibitory population, θ_e and θ_i the threshold values for firing of these excitatory, and τ the relative inhibition time, i.e., the ratio between the inhibitory and the excitatory time constants. (The excitatory time constant is, for convenience, set to unity.), Finally, $h_e(x)$ and $h_i(x)$ represent the new elements introduced to the model used in [24], i.e., stationary, localized external inputs.

The generic situation for the case without external inputs consists of two bump pairs, one narrow bump pair and one broad bump pair [24]. For spatially wide localized external inputs we find this generic picture to be unchanged. However, for strongly localized external inputs a more interesting situation emerges: here three and even four bump pairs may coexist. We next investigate the stability of these bump pairs. The two techniques used in Blomquist et al [24], namely the simplified phase-space reduction technique

(the so called *Amari* technique) and full stability analysis, are considered, and find that the Amari technique fails to produce the correct stability results in the case of strongly localized external inputs.

The paper is organized as follows: In Section 2, we discuss the two population model (1) in some detail. We show that the solution of the initial value problem of this system is globally bounded and that spatially dependent external inputs represent a symmetry breaking effect i.e the translational invariance property is violated. The existence and uniqueness of localized stationary solutions (bumps) for a given pair of threshold values subject to the spatially dependent external input are addressed in Section 4. Here and in the rest of the paper it is assumed that the firing rate functions are given by means of the Heaviside functions. In Section 5 we investigate the stability of these bumps analytically by using the Amari approach and full stability analysis. Section 6 is devoted to numerical simulations, where the time evolution of localized structures are investigated by using a fourth order Runge-Kutta method. Section 7 contain a summary of the results and an outlook. Appendix A contains the detailed derivation of the growth rate equations in the full stability analysis in Section 5, Appendix B gives the description of the numerical code underlying the numerical simulations of Section 6, while Appendix C contains the technical details underlying the discussion on the discrepancy between the Amari analysis and full stability analysis.

2. Model

The model described by (1) can more compactly be written as

$$\frac{\partial u_e}{\partial t} = -u_e + \omega_{ee} \otimes P_e(u_e - \theta_e) - \omega_{ie} \otimes P_i(u_i - \theta_i) + h_e \tag{2a}$$

$$\tau \frac{\partial u_i}{\partial t} = -u_i + \omega_{ei} \otimes P_e(u_e - \theta_e) - \omega_{ii} \otimes P_i(u_i - \theta_i) + h_i \tag{2b}$$

where the operator $\otimes$ in (2) denotes the spatial convolution integral given by

$$(f \otimes g)(x) = \int_{-\infty}^{\infty} f(x - x')g(x')dx' \ . \tag{3}$$

A schematic illustration of our two-population model is given in Fig. 1.

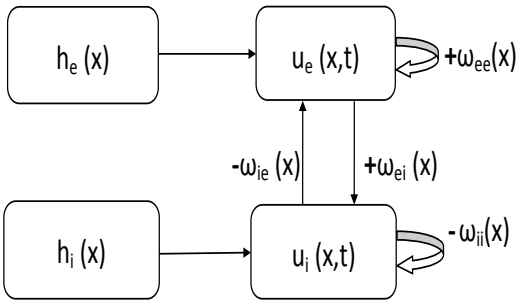

Figure 1: Sketch of the two-population neural-field model (2). An excitatory and inhibitory neuron population with space- and time-dependent activity levels $u_e(x,t)$ and $u_i(x,t)$ are driven by spatially structured external inputs $h_e(x)$ and $h_i(x)$, respectively. The populations are intra- and interconnected with distance-dependent connectivity functions $\omega_{mn}(x)$ $(m,n \in \{e,i\})$.

In the model the conversion of population activities u_e and u_i to population firing rates is done by means of the *firing-rate function* P_m $(m = e,i)$ which we in this study model as Heaviside step functions,

$$P_m(x) = \Theta(x) = \begin{cases} 0, & x < 0 \\ 1, & x \geq 0 \end{cases} \tag{4}$$

Further, the *threshold values* are assumed to be between zero and one, i.e., $0 < \theta_m \leq 1\,(m = e,i)$. The *connectivity functions* $\omega_{mn}\,(m,n = e,i)$ model the synaptic connection strength $(m \to n)$ in the network. These functions are assumed to be positive, real valued, bounded, symmetric, normalized $(\int_{-\infty}^{\infty} \omega_{mn}(x)dx = 1)$ and parameterized by the *synaptic footprints* σ_{mn}, i.e.,

$$\omega_{mn}(x) = \frac{1}{\sigma_{mn}} \Phi_{mn}(\xi_{mn}), \quad \xi_{mn} = \frac{x}{\sigma_{mn}} \tag{5}$$

Here Φ_{mn} is a dimensionless scaling function which in the present study is chosen to be a Gaussian, i.e.,

$$\Phi_{mn}(\xi_{mn}) = \frac{1}{\sqrt{\pi}} e^{-\xi_{mn}^2} \tag{6}$$

Parameters	σ_{ee}	σ_{ei}	σ_{ie}	σ_{ii}	A_e	A_i	ρ_e	ρ_i	θ_e	θ_i
Set A	0.35	0.48	0.60	0.69	0.19	0.7	0.065	0.060	0.12	0.08
Set B	0.35	0.48	0.60	0.69	0.25	0.7	0.065	0.060	0.12	0.08
Set C	0.35	0.48	0.60	0.69	0.22	0.7	0.065	0.060	0.12	0.08

Table 1: Set of parameters used as examples for different number of BPs, where σ_{mn} for $(m, n = e, i)$ represent synaptic footprints and θ_m threshold values. The parameters A_m and ρ_m for $m = e, i$ represent the amplitude and width, respectively of the external input function $h_m(x)$ given by (7). The parameter sets A, B and C are found to generate two, three and four bump pairs, respectively.

Also the functions $h_m(x)\,(m = e, i)$ describing the stationary and localized external inputs are modeled as Gaussians, i.e.,

$$h_m(x) = A_m\, e^{-(x/\rho_m)^2} \tag{7}$$

where A_m and ρ_m describe the amplitude and width, respectively.

The net excitatory activity is expressed by (2a) where $\omega_{ee} \otimes P_e(u_e - \theta_e)$ models self-interaction within the excitatory population, while the term $\omega_{ie} \otimes P_i(u_i - \theta_i)$ represents the dampening effect of the inhibitory neurons on the excitatory population. Similarly, the activity in the inhibitory population is modeled by equation (2b) where the term $\omega_{ei} \otimes P_e(u_e - \theta_e)$ represents the excitation provided by the excitatory population while the term $\omega_{ii} \otimes P_i(u_i - \theta_i)$ accounts for self-inhibition. Notice that the trivial state $u_e = 0$, $u_i = 0$ is not a solution of the system (2) unless the external input h_m is zero. Also, with no coupling in the network, stationary solutions are given by the external input functions, i.e., $U_e(x) = h_e(x)$ and $U_i(x) = h_i(x)$, and if the amplitudes A_m are smaller than the threshold there will be no firing at all.

In the present study our analytical findings will be illustrated by numerical examples, and the three parameter sets used are listed in Table 1.

3. Boundedness property

In Potthast et al [32] the wellposedness problem of a the initial value problem of the one-population Wilson-Cowan model is studied. Based on the same type of arguments as presented in Potthast et al [32] we can conclude that the initial value problem of (2) is globally wellposed. Notice also that

our model according to Faye et al [33] is globally wellposed in the space of quadratic integrable functions.

Here we study the boundedness property of the solutions to the system (2). We proceed as follows: Let V_m (m=e,i) denote the initial condition of this system. We prove that the solutions of the initial value problem (2) are uniformly bounded provided both the initial conditions and the external input functions are bounded and continuous. The proof of this fact proceeds in the same way as in [24, 32]. First, introduce the net activity levels

$$v_e(x,t) = u_e(x,t) - h_e(x) \tag{8a}$$

$$v_i(x,t) = u_i(x,t) - h_i(x) \tag{8b}$$

The evolution equations for v_e and v_i are then given by

$$\frac{\partial v_e}{\partial t} = -v_e + \omega_{ee} \otimes P_e(v_e - \tilde{\theta}_e) - \omega_{ie} \otimes P_i(v_i - \tilde{\theta}_i) \tag{9a}$$

$$\tau \frac{\partial v_i}{\partial t} = -v_i + \omega_{ei} \otimes P_e(v_e - \tilde{\theta}_e) - \omega_{ii} \otimes P_i(v_i - \tilde{\theta}_i) \tag{9b}$$

where $\tilde{\theta}_e$ and $\tilde{\theta}_i$ are spatial dependent shifted threshold values:

$$\tilde{\theta}_e(x) = \theta_e - h_e(x) \ , \ \tilde{\theta}_i(x) = \theta_i - h_i(x) \tag{10}$$

The normalization condition imposed on ω_{mn} and together with (4) imply the uniform bounds of the nonlocal terms in (9):

$$0 \leq [\omega_{mn} \otimes P_m(v_m - \tilde{\theta}_m)](x,t) \leq 1 \tag{11}$$

for all x and t. Hence we obtain the explicit bounds for the solution v_e and v_i of (9),

$$(\tilde{V}_e(x) + 1)\exp(-t) - 1 \leq v_e(x,t) \leq (\tilde{V}_e(x) - 1)\exp(-t) + 1 \tag{12a}$$

$$(\tilde{V}_i(x) + 1)\exp(-t/\tau) - 1 \leq v_i(x,t)) \leq (\tilde{V}_i(x) - 1)\exp(-t/\tau) + 1 \tag{12b}$$

by proceeding in the same way as in [24, 32]. Here

$$\tilde{V}_m(x) = V_m(x) - h_m(x) \ \ , \ \ m \in \{e,i\} \tag{13}$$

are the initial conditions for the system (9). Then, by restoring to the original variables, we deduce the bounds for the solutions u_e and u_i

$$L_m(x,t) \leq u_m(x,t) \leq R_m(x,t) \ , \ \ m \in \{e,i\} \tag{14}$$

This boundedness feature is demonstrated in the Fig. 2, where the bounding functions L_m and R_m are represented by green and blue dashed curves and are given as:

$$L_e(x,t) = (V_e(x) - h_e(x) + 1)\exp(-t) - 1 + h_e(x) \tag{15a}$$

$$R_e(x,t) = (V_e(x) - h_e(x) - 1)\exp(-t) + 1 + h_e(x) \tag{15b}$$

$$L_i(x,t) = (V_i(x) - h_i(x) + 1)\exp(-t/\tau) - 1 + h_i(x) \tag{15c}$$

$$R_i(x,t) = (V_i(x) - h_i(x) - 1)\exp(-t/\tau) + 1 + h_i(x) \tag{15d}$$

Boundedness of h_e and h_i thus implies the boundedness of the component functions u_e and u_i. We also observe that if

$$h_m(x) - 1 \leq V_m(x) \leq h_m(x) + 1 \ , \ \ m \in \{e,i\} \tag{16}$$

for all x, then

$$h_m(x) - 1 \leq u_m(x,t) \leq h_m(x) + 1 \ , \ \ m \in \{e,i\} \tag{17}$$

uniformly in t. Notice that the arguments presented here hold true also in multiple spatial dimensions or when other types of external input functions and firing rate functions are considered.

4. Existence and uniqueness of single bumps

In this section we will investigate the existence and uniqueness of localized stationary symmetric solutions (so called single bump solutions) of the system (2) by generalizing the arguments presented by Blomquist et al [24] and Pinto et al [15]. Just as in [24] we must separate the existence issue from the uniqueness issue. The existence issue consists of determining the set of threshold values for firing which produce bumps solutions of system (2). In contrast with that the uniqueness issue is a local problem and it can be posed as follows: Assume that a bump solution exists. Then we determine the conditions for having one to one correspondence between the bump solutions and the threshold values.

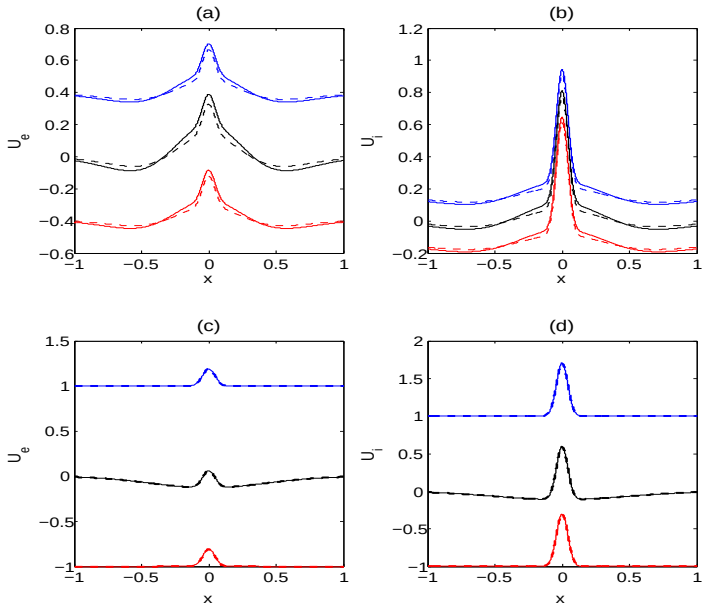

Figure 2: Example on the boundedness of bumps solution to (2) for the parameters set A in Table 1. First and second row correspond to times $t = 0.5$ and $t = 80$, respectively, while first column ((a) and (c)) represents excitatory, while second column ((b) and (d)) stands for the inhibitory activity and its bounds. Solid curves represent broad, while the dashed curves stand for narrow pulses and its bounds. The black, red and blue curves represent the activity levels, lower bounds and upper bounds respectively for $\tau = 3.127$.

4.1. Existence of single bumps

We look for time independent, spatially symmetric and localized solutions of (2) i.e. we assume that $u_m(x,t) = U_m(x), m = e, i$ where U_e and U_i are functions satisfying the following list of properties:

1) $U_m(x) = U_m(-x)$.

2) $\lim_{|x|\to\infty} U_m(x) = \lim_{|x|\to\infty} h_m(x) = 0$.

3) There exist unique points $a, b > 0$, such that $U_e(\pm a) = \theta_e$ and $U_i(\pm b) = \theta_i$ with

$$U_e(x) > \theta_e \text{ for } |x| < a \ , \quad U_e(x) < \theta_e, \quad \text{for } |x| > a \tag{18a}$$

$$U_i(x) > \theta_i \ \text{ for } |x| < b \ , \ \ U_i(x) < \theta_i, \ \ \text{for } |x| > b \tag{18b}$$

The stationary solutions of (2) are referred to as *single bump solutions*. The parameters a, b denote the widths of the excitatory and the inhibitory pulses, respectively. According to the conditions $1) - 3)$, the expressions for $U_e(x)$ and $U_i(x)$ are given as

$$U_e(x) = W_{ee}(x+a) - W_{ee}(x-a) - W_{ie}(x+b) + W_{ie}(x-b) + h_e(x) \tag{19a}$$

$$U_i(x) = W_{ei}(x+a) - W_{ei}(x-a) - W_{ii}(x+b) + W_{ii}(x-b) + h_i(x) \tag{19b}$$

Here $W_{mn}(x)$ is the integral defined as

$$W_{mn}(x) = \int_0^x \omega_{mn}(y)dy \tag{20}$$

Notice that W_{mn} is an odd function. By following the above assumptions, the conditions for a stationary symmetric solution are

$$f_e(a,b) = \theta_e \quad \text{and} \quad f_i(a,b) = \theta_i \tag{21}$$

where f_e and f_i are given as

$$f_e(a,b) = W_{ee}(2a) - W_{ie}(a+b) + W_{ie}(a-b) + h_e(a) \tag{22a}$$

$$f_i(a,b) = W_{ei}(a+b) - W_{ei}(b-a) - W_{ii}(2b) + h_i(b) \tag{22b}$$

In order to prove the existence of bumps, we need to find threshold values θ_m in the interval $(0,1]$, for which the system (2) and the equation (21) possess a solution. We proceed in the same way as in [24] by translating the problem into a mapping problem. We introduce the two subsets Σ of $\mathbb{R}^2$ and I in the (θ_e, θ_i) plane, which are defined as

$$I = (0,1] \times (0,1] \ , \ \ \Sigma = \{(a,b) | a \geq 0, b \geq 0\} \tag{23}$$

We call I the *threshold value set* and Σ the *pulse width set*. We have the following existence theorem for solutions of (21):

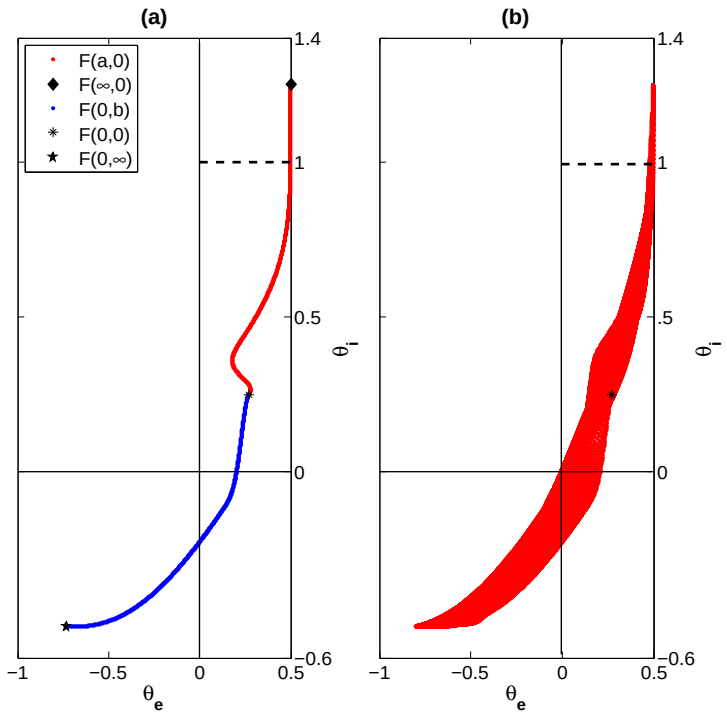

Figure 3: Mapping of the pulse-width coordinate plane to the threshold value plane showing non-empty admissible set of threshold values, where dashed lines imply $0 < \theta_m \leq 1$. **(a)** Images of the origin $a = b = 0$ $(*)$, the a-axis $(a > 0,\ b = 0)$ (red curve), the b-axis $(a = 0,\ b > 0)$ (blue curve), and the limit values $(a \to \infty, b = 0)$ $(\diamond)$ and $(a = 0, b \to \infty)$ $(\star)$. **(b)** Image of the entire pulse-width plane showing non-empty intersection with the threshold-value plane. The synaptic footprints are given by Table 1. The amplitude and width parameters of the external input functions are $(A_e, A_i) = (0.27, 0.25)$ and $(\rho_e, \rho_i) = (0.032, 0.03)$, respectively.

Theorem 1. *Let the external input functions h_m be given by (7) and assume that $(A_e, A_i) \in I$. Introduce the vector field $\underline{F} : \Sigma \to \mathbb{R}^2$ defined as*

$$\underline{\theta} = \underline{F}(\underline{a}) \tag{24}$$

where

$$\underline{F} = (f_e, f_i)^t,\ \underline{a} = (a, b)^t,\ \underline{\theta} = (\theta_e, \theta_i)^t,\ \underline{a} \in \Sigma \tag{25}$$

with f_e and f_i given as (22). Then the set $\underline{F}(\Sigma)$ is bounded and there is a subset Σ_0 of Σ such that $\underline{F}(\Sigma_0) \cap I$ is non-empty.

PROOF. We first prove that the set $\underline{F}(\Sigma)$ is bounded. Since the functions ω_{mn} are symmetric and normalized, we find the uniform bound

$$|W_{mn}(y)| \leq \frac{1}{2} \tag{26}$$

We also notice that

$$|h_e(a)| \leq A_e \ , \quad |h_i(b)| \leq A_i \tag{27}$$

Hence we get

$$|f_e(a,b)| \leq \frac{3}{2} + |A_e|, \quad |f_i(a,b)| \leq \frac{3}{2} + |A_i| \tag{28}$$

from which the boundedness of $\underline{F}(\Sigma)$ follows.

The assumptions imposed on the connectivity functions imply continuity of the anti-derivatives W_{mn} defined by (20). Since by assumption the external input functions h_m are continuous, we conclude that the vector field $\underline{F}$ is a continuous mapping. We observe that $\underline{F}(0,0) = (A_e, A_i) \in I$. Then, by continuity of $\underline{F}$ there is an open neighborhood of $(a,b) = (0,0)$ which is mapped to an open neighborhood of (A_e, A_i). We hence conclude that there is a subset Σ_0 of Σ such that $\underline{F}(\Sigma_0) \cap I$ is non-empty.

In order to illustrate in detail the mapping properties of the vector field $\underline{F}$ we proceed as follows: The image of the positive a-axis is the smooth curve $\underline{\zeta} : [0, \infty) \to \mathbb{R}^2$ with the parametrization

$$\underline{\zeta}(a) = \underline{F}(a,0) = \begin{bmatrix} f_e(a,0) \\ f_i(a,0)) \end{bmatrix} = \begin{bmatrix} W_{ee}(2a) + h_e(a) \\ 2W_{ei}(a) + A_i \end{bmatrix} \tag{29}$$

with the properties

$$\underline{\zeta}(0) = \begin{bmatrix} A_e \\ A_i \end{bmatrix}, \quad \underline{\zeta}(a \to \infty) = \begin{bmatrix} 1/2 \\ 1 + A_i \end{bmatrix} \tag{30}$$

Since $\frac{dW_{ei}}{da} = \omega_{ei}(a) > 0$, W_{ei} is a strictly increasing function of a and hence it is invertible. For a given admissible θ_i, the equation $2W_{ei}(a) + A_i = \theta_i$ has a unique solution. Hence the positive a-axis is mapped onto the graph of some smooth function g where $\theta_e = g(\theta_i)$. Differentiation yields

$$g'(\theta_i) = \frac{d\theta_e}{d\theta_i} = \frac{2\omega_{ee}(a) + h_e'(a)}{2\omega_{ei}(a)} \tag{31}$$

The numerator consists of two terms, where the first one is positive and the second one negative. The monotonicity depends sensitively on the steepness of the excitatory external input function h_e. For broad excitatory external input, the first term of the numerator will dominate, and hence the function g in this case is strictly increasing, just as in the case of no external input. In the complementary regime, with strongly localized external input function h_e, there is a θ_i-interval for which g is strictly decreasing. Based on this analysis we may expect that the most significant qualitative difference between the no-input case and the finite input case occurs for the strongly localized external parameter regime case.

Next, let us study the image of the positive b-axis under the vector field $\underline{F}$. In that case we get a smooth curve $\underline{\sigma} : [0, \infty) \to \mathbf{R}^2$ with parametrization given by

$$\underline{\sigma}(b) = \underline{F}(0, b) \begin{bmatrix} -2W_{ie}(b) + A_e \\ -W_{ii}(2b) + h_i(b) \end{bmatrix} \tag{32}$$

We observe that

$$\underline{\sigma}(0) = \begin{bmatrix} A_e \\ A_i \end{bmatrix}, \underline{\sigma}(b \to \infty) = \begin{bmatrix} -1 + A_e \\ -1/2 \end{bmatrix} \tag{33}$$

Now, since W_{ie} is a strictly increasing function of b, the equation $\theta_e = -2W_{ie}(b) + A_e$ has a unique solution for a given admissible θ_e. Hence the positive b-axis is mapped onto the graph of some smooth function: $\theta_i = G(\theta_e)$. As

$$G'(\theta_e) = \frac{d\theta_i}{d\theta_e} = \frac{2\omega_{ii}(2b) + |h_i'(b)|}{2\omega_{ie}(b)} > 0 \tag{34}$$

G is a strictly increasing function of θ_e. The whole mapping process of the boundary curves a=0, b=0 and the first quadrant of Σ is illustrated in Fig. 3.

We call the set of (θ_e, θ_i) values for which the system (21) and (22) has a solution *the admissible set of threshold values*. Hence, if $(A_e, A_i) \in I$, there exists a subset of the threshold values (θ_e, θ_i) for which the model possesses spatially symmetric solutions given by (19)-(22). Hereafter we will refer to the above theorem as the *existence theorem for bumps*. Notice that the existence theorem for bumps says that a single bump exists provided the amplitude A_m of the external inputs are small and moderate. Above certain thresholds of the amplitudes of the external inputs, no bumps exist. This should be compared to the situation without external inputs treated in Blomquist et al [24] where we always have an admissible set of threshold values i.e. we can always find threshold values producing bumps.

4.2. Uniqueness of bumps

We let the threshold values (θ_e, θ_i) belong to the set of admissible threshold values and (a_{eq}, b_{eq}) be the corresponding solution of the system (21) and (22). We assume that the connectivity functions are continuous. This implies that the component functions f_e and f_i defined by (22) are continuously differentiable. According to the inverse function theorem, $\underline{F}$ is locally one-to-one and onto, if the Jacobian of $\underline{F}$ evaluated at the $\underline{a}_{eq} = (a_{eq}, b_{eq})$ is non singular, i.e.

$$det[\frac{\partial \underline{F}}{\partial \underline{a}}](\underline{a}_{eq}) \neq 0 \tag{35}$$

Thus there will be an open neighborhood of $\underline{a}_{eq}$, which is mapped bijectively to the open neighborhood of (θ_e, θ_i) . Geometrically, the solution of the system (21) with condition (35) corresponds to a transversal intersection between the two level curves $f_e = \theta_e$ and $f_i = \theta_i$. Hence each transversal intersection of level curves $f_m = \theta_m$ corresponds to a bump solution of the system (21).

The pulse pair generation is connected to the breakdown of the transversality condition (35) in a way analogous to Blomquist et al [24] and Pinto et al [15]. We typically get two bumps pairs (BPs) for a pair of threshold values. Fig. 4 shows a numerical example on a situation with two bumps corresponding to the set of parameters A in Table 1. Here we used the same synaptic footprints and threshold values as used in [24]. The corresponding pulse width coordinates are given as in Table 6.

$$(a_1, b_1) = (0.112, 0.116),\ (a_2, b_2) = (0.180, 0.183) \tag{36}$$

For convenience, we term the pulse pair corresponding to the intersection point (a_1, b_1) as a *narrow pulse pair*, while (a_2, b_2) is referred as a *broad pulse pair*. Pulse pairs in this case are shown as blue solid curves in Fig.4.

However, the addition of spatial dependent external inputs in the model makes it possible to identify parameter regimes for which we have even three and four BPs for a given pair of threshold values. This is a qualitatively new feature, apparently with no counterpart in the case with no - or constant external inputs.

The figures 5 and 6 give a global overview over the number of BPs as a function of firing thresholds and input amplitudes, respectively. In Fig. 5,

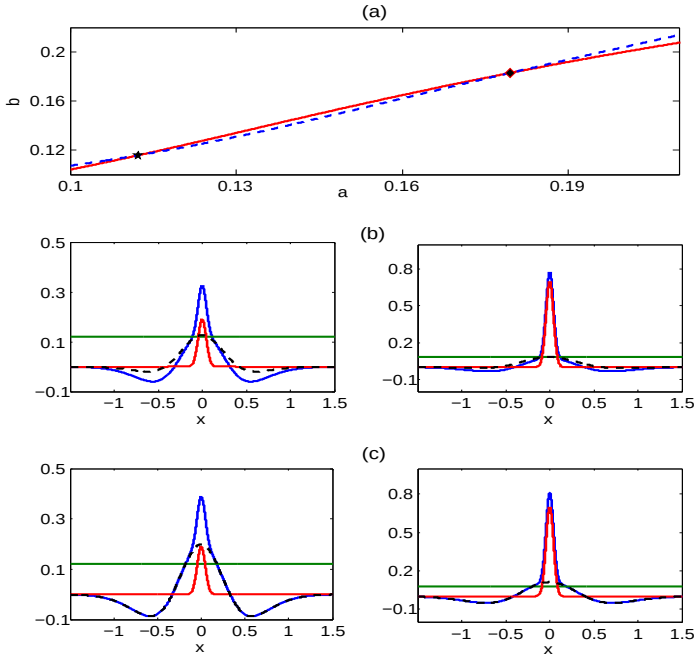

Figure 4: Effect of spatially structured external input on stationary BP solutions. **(a)** Intersections of level curves $f_e(a,b) = \theta_e$ (solid red) and $f_i(a,b) = \theta_i$ (dashed blue) illustrating the generation of two BPs in the presence of external input. **(b,c)** Excitatory (left) and inhibitory activity levels (right) for narrow (b) and broad BPs (c) with (solid blue curves) and without localized external input (dashed black curves). Green and red lines represent threshold values and external input functions, respectively. Input parameters: Parameter set A in Table 1.

we show the number of BPs in the threshold value plane keeping the amplitudes and the width parameters of the external input parameters fixed. Fig.5(a) shows the threshold value plane for the case without external inputs, i.e., $A_e = A_i = 0$. Here we recover the situation studied in [24]. Fig. 5(b) represents an example with wide external inputs and small amplitudes. It illustrates that the set of admissible threshold values emerges as a continuous deformation of the admissible threshold value set in the no input case. Qualitatively new features like three or four coexisting BPs do not exist in this situation. This result is to be expected as the no-external input case

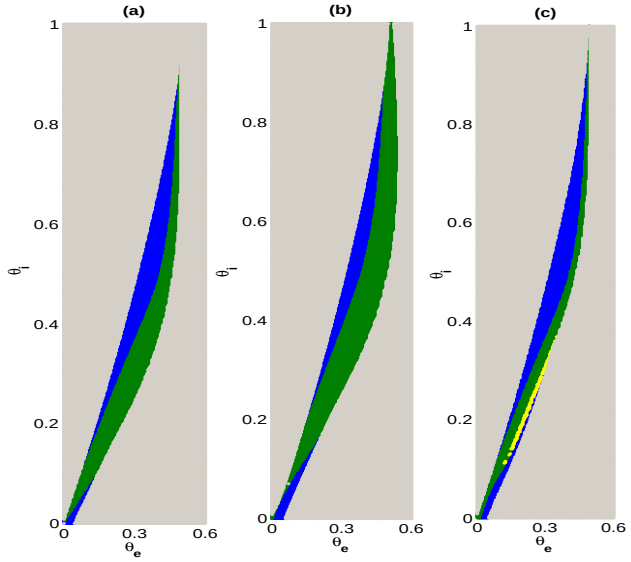

Figure 5: Number of bump solutions in the threshold-value plane, where the colors grey, green, blue and yellow represent zero, one, two and three bump solutions, respectively. **(a)** No external input. **(b)** Wide external input ($\rho_e = 0.65$, $\rho_i = 0.60$). **(c)** Localized external input ($\rho_e = 0.065$, $\rho_i = 0.060$). In **(b)** and **(c)** $A_e = 0.072$ and $A_i = 0.070$. The other parameters are as given in Table 1.

can be considered as a limiting case of the small amplitude - wide external input situation. When decreasing the width parameters of the external input functions while keeping the amplitude parameters fixed Fig.5(c), regions in the admissible part of the threshold value plane with three BPs appear. This effect is caused by the localization of the external inputs.

In Fig. 6 we identify the number of BPs as a function of the external input amplitudes for fixed widths, synaptic footprints and threshold values. As the regime of strongly localized external input appears to be the regime for which the deviation from the no-external input case is most prominent, we have chosen the width parameters of the external input functions to be

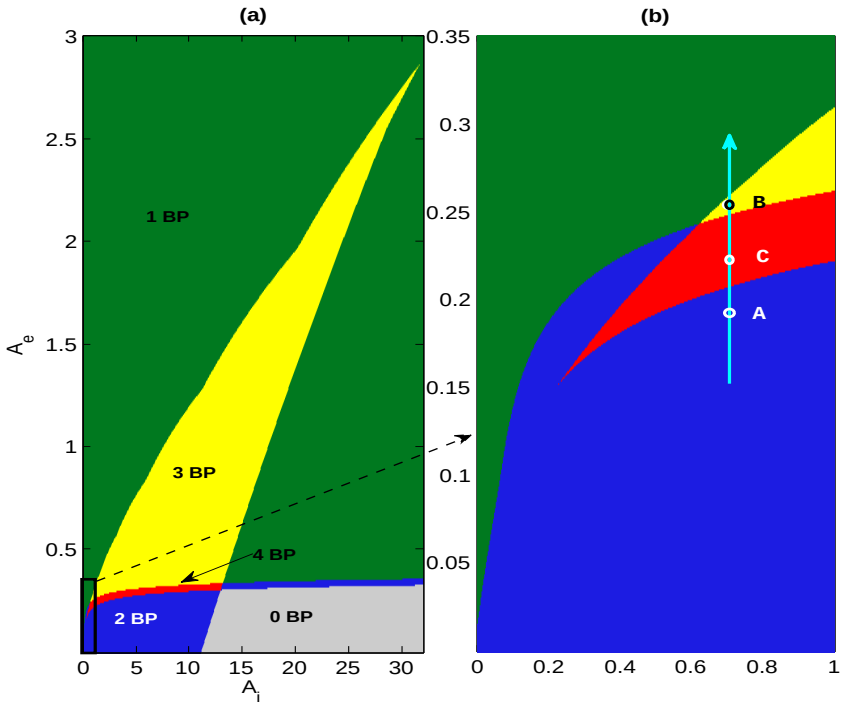

Figure 6: **(a)** Dependence of the number of bump-pair (BP) solutions on the amplitudes A_e, A_i of the external input (7). **(b)** Magnified view of the region marked by the black rectangle in (a). Marks on the directed line segment correspond to different numbers of BP scenarios displayed in Figs. 4, 8 and 9. The corresponding width coordinates, threshold values and synaptic footprints are given in Table 1. The points A, B and C correspond to the parameter sets A, B and C in Table 1, respectively.

the same as those used in Fig. 5(c). We observe regimes with both three and four BPs. In the following we focus on representative examples of three and four BPs solutions (points B and C in Fig. 6b) by using parameter sets B and C in Table 1, respectively. For parameter set B of Table 1, three pairs of solutions of (21) with pulse width coordinates

$$(a_1, b_1) = (0.080, 0.096) \tag{37a}$$

$$(a_2, b_2) = (0.100, 0.108) \tag{37b}$$

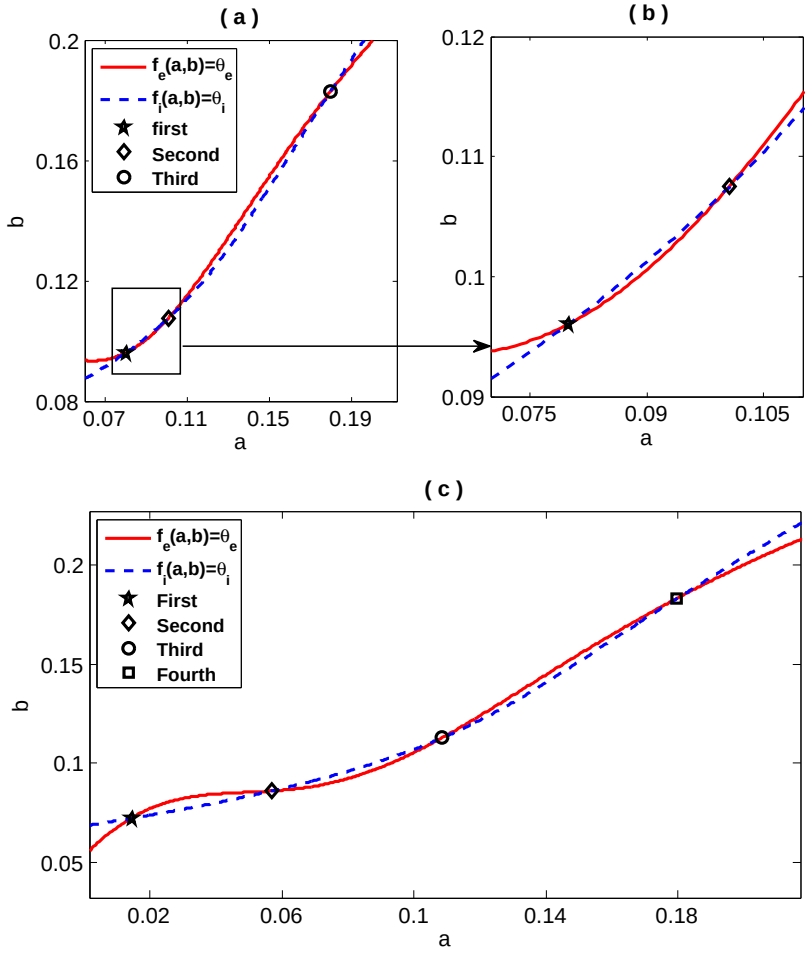

Figure 7: Intersections between the level curves $f_e = \theta_e$ (solid red lines) and $f_i = \theta_i$ (dashed blue lines) representing three (a,b) and four BP solutions (c). **(a)** Three BP scenario (cf. Fig. 8; parameter set B in Table 1). **(b)** Magnified view of the rectangular region marked in (a). **(c)** Four BP scenario (cf. Fig. 9; parameter set C in Table 1).

$$(a_3, b_3) = (0.180, 0.183) \tag{37c}$$

exist. The corresponding intersections of level curves $f_e = \theta_e$ and $f_i = \theta_i$ and BPs are shown in Fig. 7a, Fig. 7b and Fig. 8, respectively.

For the parameter set C, the equations (21) have four solutions with

$$(a_1, b_1) = (0.014, 0.072), \quad (a_2, b_2) = (0.057, 0.086) \tag{38a}$$

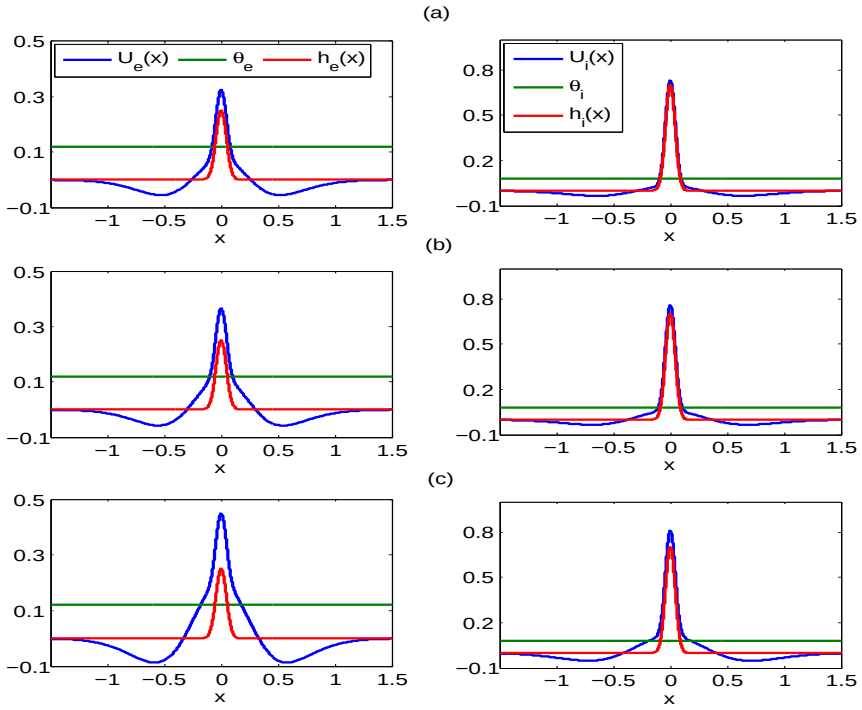

Figure 8: Three BP scenario. Excitatory (left column) and inhibitory (right column) activity (blue lines) for the BPs corresponding to the **(a)** first, **(b)** second, and **(c)** third level-curve intersection in Fig. 7a. Red and green lines represent external input and threshold values, respectively. The input parameters: Parameter set B in Table 1.

$$(a_3, b_3) = (0.108, 0.113), \quad (a_4, b_4) = (0.180, 0.183) \tag{38b}$$

The level curves intersections producing these solutions are displayed in Fig. 7(c) and the corresponding pulse pairs in this case are shown in Fig. 9.

5. Stability analysis

In this section we will investigate the stability of the bumps using both the Amari approach and the full linearized stability analysis.

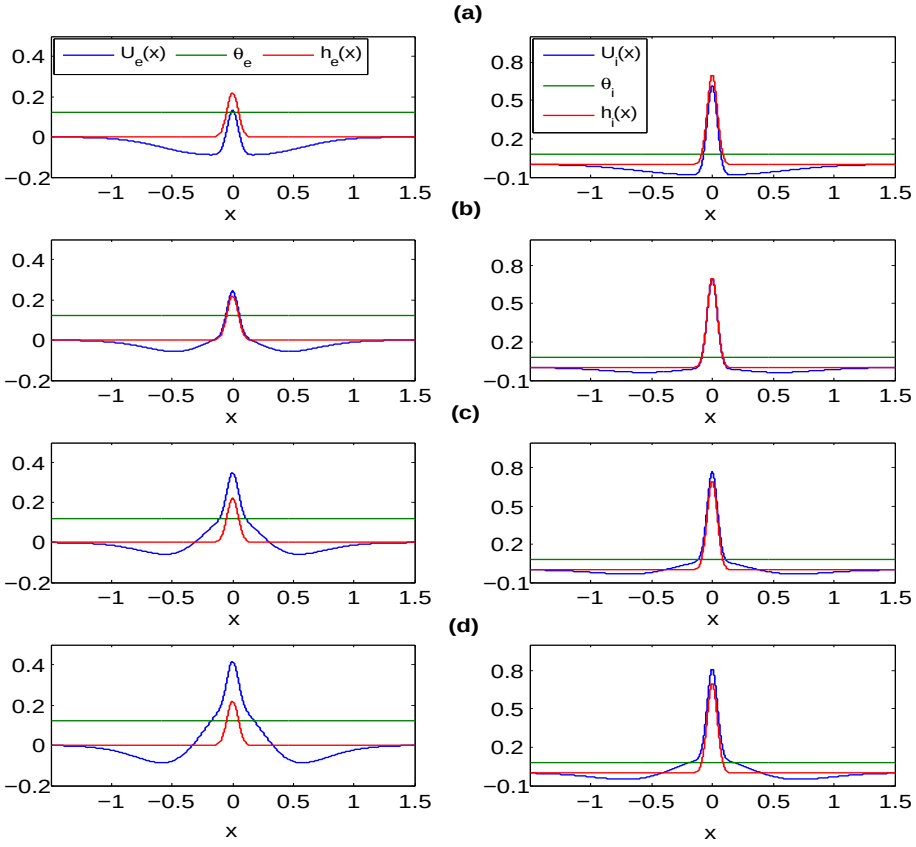

Figure 9: Four BP scenario. Excitatory (left column) and inhibitory (right column) activity (blue lines) for the BPs corresponding to the **(a)** first, **(b)** second, **(c)** third, and **(d)** fourth level-curve intersection in Fig. 7c. Red and green lines represent external input and threshold values, respectively. Input parameters: Parameter set C in Table 1.

5.1. The Amari approach

A pulse pair (U_e, U_i) is identified with the intersection point (a, b) between the level curves

$$f_e(a,b) = \theta_e \ , \quad f_e(a,b) = \theta_i \tag{39}$$

This is the starting point of the simplified stability analysis originally worked out by Amari [9] and later on used by Pinto et al [15] and Blomquist et al [24]. This approach presupposes that the stability of the pulses can be inferred from the stability of the intersection point (a, b).

To analyze the stability of bumps, it is necessary to prescribe the dynamical evolution of the intersection point (a, b) in a way consistent with the system (2). First assume that (θ_e, θ_i) belongs to the admissible threshold value set, which imply that the level curves will intersect at least at one point (a_{eq}, b_{eq}) in the pulse width set $\sum$. In order to describe the time evolution of small perturbations $(a(t), b(t))$ to (a_{eq}, b_{eq}), we make the following assumptions:

1. The perturbed pulses satisfy the same threshold-value conditions as the stationary pulses, i.e,

$$u_e(a(t), t) = \theta_e \quad , \quad u_i(b(t), t) = \theta_i \tag{40}$$

2. The slopes of the perturbed pulses at the crossing points $(a(t), b(t))$ are identical to the slopes at (a_{eq}, b_{eq}), i.e

$$\partial_x u_e(a, t) \approx U_e'(a_{eq}) \quad , \quad \partial_x u_i(b, t) \approx U_i'(b_{eq}) \tag{41}$$

Since $U_e'(a_{eq}) < 0$ and $U_i'(b_{eq}) < 0$, we have

$$\partial_x u_e(a, t) \approx -|U_e'(a_{eq})| \quad , \quad \partial_x u_i(b, t) \approx -|U_i'(b_{eq})| \tag{42}$$

The approximations (41) and (42) are referred to as the *static slope approximation*. By differentiating (40) with respect to t and using (2), (22), (40) and (42) we get

$$|U_e'(a_{eq})|\frac{da}{dt} = f_e(a, b) - \theta_e \tag{43a}$$

$$\tau|U_i'(b_{eq})|\frac{db}{dt} = f_i(a, b) - \theta_i \tag{43b}$$

The equilibrium points of the system (43) determine the widths of the unperturbed bumps. The system (43) is a 2D autonomous system which constitutes the basis for the stability analysis. In order to determine the stability of $\underline{a}_{eq}$, we compute the Jacobian of (43) at $\underline{a}_{eq}$ and eigenvalues. The Jacobian is given by

$$\boldsymbol{J}_A = \begin{bmatrix} \beta_A & -\eta_A \\ \frac{1}{\tau}\mu_A & -\frac{1}{\tau}\alpha_A \end{bmatrix} \tag{44}$$

where the entries β_A, η_A, μ_A and α_A are defined as

$$\beta_A = \frac{1}{|U_e'(a_{eq})|}\{2\omega_{ee}(2a_{eq}) - \omega_{ie}(a_{eq}+b_{eq}) + \omega_{ie}(a_{eq}-b_{eq}) + h_e'(a_{eq})\} \quad (45a)$$

$$\eta_A = \frac{1}{|U_e'(a_{eq})|}\{\omega_{ie}(a_{eq}+b_{eq}) + \omega_{ie}(a_{eq}-b_{eq})\} \quad (45b)$$

$$\mu_A = \frac{1}{|U_i'(b_{eq})|}\{\omega_{ei}(a_{eq}+b_{eq}) + \omega_{ei}(b_{eq}-a_{eq})\} \quad (45c)$$

$$\alpha_A = \frac{1}{|U_i'(b_{eq})|}\{2\ \omega_{ii}(2b_{eq}) - \omega_{ei}(a_{eq}+b_{eq}) + \omega_{ei}(b_{eq}-a_{eq}) + h_i'(b_{eq})\} \quad (45d)$$

The eigenvalues λ of the Jacobian $\boldsymbol{J}_A$ satisfy the quadratic equation

$$\tau\lambda^2 + \lambda(\alpha_A - \tau\beta_A) + \gamma_A = 0 \quad (46)$$

with

$$\gamma_A = \mu_A\eta_A - \alpha_A\beta_A \quad (47)$$

According to standard theory for 2D autonomous dynamical systems, the stability issue can be resolved by means of the invariants of the $\boldsymbol{J_A}$ i.e the trace and determinant

$$T \ = tr(\boldsymbol{J}_A) = \beta_A - \tfrac{\alpha_A}{\tau} \ , \ D = det(\boldsymbol{J}_A) = \tfrac{\gamma_A}{\tau} \quad (48)$$

respectively.

When the parameter $\gamma_A < 0$, we have $det(\boldsymbol{J}_A) < 0$, which corresponds to a saddle point instability. In order to discuss the complementary regime $\gamma_A > 0$ ($\Leftrightarrow det\boldsymbol{J}_A > 0$), we introduce the critical relative inhibition time τ_{cr} defined as

$$\tau_{cr} = |\alpha_A|/|\beta_A| \quad (49)$$

We have stability whenever T given by (48) is strictly negative. This happens in the following three scenarios

1.) $\alpha_A > 0$ and $\beta_A < 0$ for all values of τ

2.) $\alpha_A > 0$ and $\beta_A > 0$, for $\tau < \tau_{cr}$

3.) $\alpha_A < 0$ and $\beta_A < 0$ for $\tau > \tau_{cr}$

The cases with $T > 0$, $det(\boldsymbol{J}_A) > 0$ correspond to instability. They occur in one of the following three cases if

$\gamma_A < 0$			Saddle point instability
$\gamma_A > 0$	$\alpha_A > 0$	$\beta_A < 0$	Stability for all τ
	$\alpha_A > 0$	$\beta_A > 0$	Stability if $\tau < \tau_{cr}$, instability for $\tau > \tau_{cr}$
	$\alpha_A < 0$	$\beta_A < 0$	Stability if $\tau > \tau_{cr}$, instability if $\tau < \tau_{cr}$
	$\alpha_A < 0$	$\beta_A > 0$	Instability

Table 2: Stability results according to the Amari approach ($\tau_{cr} = |\alpha_A|/|\beta_A|$)

1.) $\alpha_A < 0$ and $\beta_A > 0$ for all values of τ

2.) $\alpha_A > 0$ and $\beta_A > 0$, for $\tau > \tau_{cr}$

3.) $\alpha_A < 0$ and $\beta_A < 0$ for $\tau < \tau_{cr}$

The classification scheme for the stability is summarized in Table 2

Notice that the parameters α_A, $\beta_A > 0$ for no or constant external inputs, ($i.e$ $h_e'(a_{eq}) = 0$ and $h_i'(b_{eq}) = 0$). For spatially dependent external inputs, the parameters α_A and β_A are not sign definite. Hence the stability discussion becomes more involved in the present case as compared with the case treated in Blomquist et al [24].

We close this subsection by studying the validity of the Amari approach. In Fig. 10 we have plotted the slope parameter $S_i(t) \equiv \partial_x u_i(b,t)$ as a function of time in the vicinity of $t = 0$ in a case with strongly localized external inputs and in a case with wide external inputs. The initial condition is chosen to be a narrow bump. The computation underlying this plot is based on the numerical scheme worked out in appendix Appendix B. This plot confirms numerically that the static slope approximation (41) represents a poor approximation in the strongly localized case (solid blue curve), whereas the slope remains almost constant on the actual time interval and hence approximates fairly well in the case of wide external inputs (solid red curve). This result is indeed reflected in the comparison between the Amari approach and the full stability analysis elaborated in subsection 5.3.

5.2. Full stability analysis

In this section we will discuss the stability of bumps by using the standard linearization procedure in a way similar to the one used by Blomquist et al

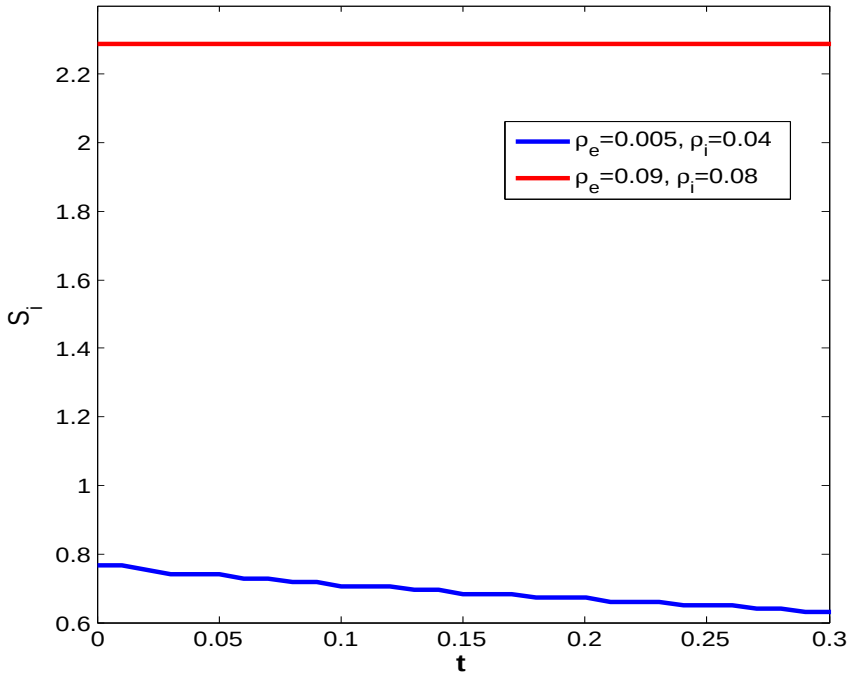

Figure 10: Validity of the static slope approximation (41). The slope parameter $S_i(t) \equiv \partial_x u_i(b,t)$ for the case of wide external input (solid red curve) and strongly localized input (solid blue curve). The input parameters are $\tau = 0.24$ while the other input parameters (except the width parameters ρ_e and ρ_i) are as in parameter set A in Table 1

[24] and Pinto et al [15]. We start out by linearizing the system of equations (2) about the bump solutions $(U_e(x), U_i(x))$. Let $U_e(x)$ and $U_i(x)$ be spatially symmetric and time independent solutions of (2), i.e.

$$U_e = \omega_{ee} \otimes \Theta(U_e - \theta_e) - \omega_{ie} \otimes \Theta(U_i - \theta_i) + h_e \tag{50a}$$

$$U_i = \omega_{ei} \otimes \Theta(U_e - \theta_e) - \omega_{ii} \otimes \Theta(U_i - \theta_i) + h_i \tag{50b}$$

Introduce the perturbed state

$$u_e(x,t) = U_e(x) + \kappa(x,t) \tag{51a}$$

$$u_i(x,t) = U_i(x) + \chi(x,t) \tag{51b}$$

The Taylor expansion of the Heaviside function Θ about the equilibrium state $(U_e,\ U_i)$ yields

$$\Theta(U_e - \theta_e + \ \kappa) = \Theta(U_e - \theta_e) + \kappa\ \delta(U_e - \theta_e) + \cdots \tag{52a}$$

$$\Theta(U_i - \theta_i + \ \chi) = \Theta(U_i - \theta_i) + \chi\ \delta(U_i - \theta_i) + \cdots \tag{52b}$$

where δ denotes the Dirac delta function. Since $|\kappa| \ll |U_e - \theta_e|$ and $|\chi| \ll |U_i - \theta_i|$ by assumption, we only retain the two lowest order terms in the expansions.

Using (52) and (51) in (2), the linearized perturbed system is

$$\kappa_t = -\kappa + \omega_{ee}\ \otimes \delta(\ (U_e - \theta_e\ )\ \kappa) - \omega_{ie} \otimes \delta(\ (U_i - \theta_i\ )\chi) \tag{53a}$$

$$\tau\chi_t = -\chi + \omega_{ei} \otimes \delta(\ (U_e - \theta_e\ )\kappa) - \omega_{ii} \otimes \delta(\ (U_i - \theta_i\ )\chi) \tag{53b}$$

We then, look for solutions of the perturbed system on the form

$$\kappa(x,t) = e^{\lambda t}\kappa_1(x) \qquad \chi(x,t) = e^{\lambda t}\chi_1(x) \tag{54}$$

Here λ plays the role of growth rate $((Re(\lambda) > 0))$ or decay rate $((Re(\lambda) < 0))$ of the perturbation imposed on the stationary pulse pair defined by (50).

We notice that the system (53) has the same form as the linearized perturbed system derived in [24] for the full stability analysis in the non-external input case. Hence, the derivation of the characteristic equations for λ proceeds in the same way as in Blomquist et al [24]. We end up with two characteristic polynomials (See Appendix A).

$$\tau\lambda^2 + (\alpha_L - \beta_L\tau)\lambda + \gamma_L = 0 \tag{55}$$

$$\tau\lambda^2 + (\alpha'_L - \beta'_L\tau)\lambda + \gamma'_L = 0 \tag{56}$$

Here the coefficients are given as

$$\alpha_L = C_3 + C_4 + 1,\ \beta_L = A_1 + A_2 - 1 \tag{57a}$$

$$\gamma_L = (C_1 + C_2)(A_3 + A_4) - (C_3 + C_4 + 1)(A_1 + A_2 - 1) \tag{57b}$$

$$\alpha'_L = C_3 - C_4 + 1,\ \beta'_L = A_1 - A_2 - 1 \tag{58a}$$

$$\gamma'_L = (C_1 - C_2)(A_3 - A_4) - (C_3 - C_4 + 1)(A_1 - A_2 - 1) \tag{58b}$$

where

$$A_1 = \frac{\omega_{ee}(0)}{|U'_e(a_{eq})|},\ A_2 = \frac{\omega_{ee}(2a_{eq})}{|U'_e(a_{eq})|},\ A_3 = \frac{\omega_{ie}(a_{eq} - b_{eq})}{|U'_e(a_{eq})|} \tag{59a}$$

$$A_4 = \frac{\omega_{ie}(a_{eq} + b_{eq})}{|U'_e(a_{eq})|},\ \ C_1 = \frac{\omega_{ei}(a_{eq} - b_{eq})}{|U'_i(b_{eq})|},\ \ C_2 = \frac{\omega_{ei}(a_{eq} + b_{eq})}{|U'_i(b_{eq})|} \tag{59b}$$

$$C_3 = \frac{\omega_{ii}(0)}{|U'_i(b_{eq})|},\ C_4 = \frac{\omega_{ii}(2b_{eq})}{|U'_i(b_{eq})|} \tag{59c}$$

The subscript L indicates that the stability analysis is based on the full linearization procedure of the model presented. For the sake of completeness we give a detailed derivation of (55) and (56) in Appendix A. According to the standard stability theory, we have stability if all eigenvalues of the characteristic equations have negative real part and instability if at least one of the eigenvalues has non-negative real part. The eigenvalues λ can be expressed in terms of the traces ($tr(\mathbf{M}_i)$) and the determinant ($det(\mathbf{M}_i)$) of the block diagonal matrices $\mathbf{M}_1$ and $\mathbf{M}_2$ (see Appendix A). For convenience , let us introduce the notations

$$T_1 = tr(\mathbf{M}_1) = \beta_L - \frac{\alpha_L}{\tau}, \quad \gamma_L = \tau\ det(\mathbf{M}_1) \tag{60}$$

$$T_2 = tr(\mathbf{M}_2) = \beta'_L - \frac{\alpha'_L}{\tau}, \quad \gamma'_L = \tau\ det(\mathbf{M}_2) \tag{61}$$

The stability of the bumps can now be analyzed by means of parameters α_L,α'_L, β_L,β'_L,γ_L and γ'_L. Notice that $\alpha_L, \alpha'_L > 0$. We hence introduce the critical time constants τ_{cr} and τ'_{cr} defined as

$$\tau_{cr} = \frac{\alpha_L}{|\beta_L|}\ \ ,\ \ \tau_{cr'} = \frac{\alpha'_L}{|\beta'_L|} \tag{62}$$

Tables 3 and 4 summarize the relationship between the parameters involved and the properties of the roots of (55) and (56). A saddle point instability occurs if at least one of the parameters γ_L and γ'_L is negative. In the complementary regime, i.e when both γ_L and γ'_L are strictly positive, we have to take into the consider the signs of the parameters β_L and β'_L. We summarize the full stability results in table 5 for the case $\gamma_L, \gamma'_L > 0$. Here $\tau''_{cr} = min(\tau_{cr}, \tau'_{cr})$

$\gamma_L < 0$		$\lambda_- < 0 < \lambda_+$
$\gamma_L > 0$	$\beta_L < 0$	$Re(\lambda_\pm) < 0$ for all τ
	$\beta_L > 0$	$Re(\lambda_\pm) < 0$ for $\tau < \tau_{cr}$
		$Re(\lambda_\pm) > 0$ for $\tau > \tau_{cr}$

Table 3: The roots of (55) ($\tau_{cr} = \frac{\alpha_L}{|\beta_L|}$)

$\gamma'_L < 0$		$\lambda'_- < 0 < \lambda'_+$
$\gamma'_L > 0$	$\beta'_L < 0$	$Re(\lambda'_\pm) < 0$ for all τ
	$\beta'_L > 0$	$Re(\lambda'_\pm) < 0$ for $\tau < \tau'_{cr}$
		$Re(\lambda'_\pm) > 0$ for $\tau > \tau'_{cr}$

Table 4: The roots of (56). ($\tau_{cr'} = \frac{\alpha'_L}{|\beta'_L|}$)

$\beta_L < 0$	$\beta'_L < 0$	Stability for all τ values
	$\beta'_L > 0$	Stability(instability) for $\tau < \tau'_{cr} (\tau > \tau'_{cr})$
$\beta_L > 0$	$\beta'_L < 0$	Stability (instability) for $\tau < \tau_{cr} (\tau > \tau_{cr})$
	$\beta'_L > 0$	Stability (instability) for $\tau < \tau''_{cr} (\tau > \tau''_{cr})$.

Table 5: Stability results using full stability analysis for $\gamma_L, \gamma'_L > 0$

5.3. Amari analysis vs. full stability analysis

In Appendix C we prove the following relationships between the parameters $(\alpha_A, \beta_A, \gamma_A)$ in the growth rate equation (46) obtained in the Amari analysis and the parameters $(\alpha_L, \beta_L, \gamma_L)$ in the growth rate equation (55) (corresponding to the symmetric part of the perturbations in the full stability analysis):

1.) $\alpha_L = \alpha_A - \frac{2h'_i(b_{eq})}{|U'_i(b_{eq})|}$

2.) $\beta_L = \beta_A$

3.) $\gamma_A = \gamma_L - Q, \quad Q \equiv 2\frac{h'_i(b_{eq})}{|U'_i(b_{eq})|}(2A_2 - A_4 + A_3) + 2\frac{h'_i(b_{eq}).h'_e(a_{eq})}{|U'_i(b_{eq})|.|U'_e(a_{eq})|}$

Therefore the present Amari analysis and the full stability analysis give different results for spatial dependent external inputs. This result is qualitatively completely different from the result obtained in Folias et al [19], where it is shown that the Amari analysis yields the same predictions as the full-stability

Pulse width coordinates	Stability parameters	Stability results
$(a_1, b_1) = (0.112, 0.116)$	$\alpha_A = 0.499, \beta_A = 1.89$ $\gamma_A = 2.30, \tau_{cr} = 0.258$	Stability /(instability) for $\tau < \tau_{cr}/(\tau > \tau_{cr})$
$(a_2, b_2) = (0.180, 0.183)$	$\alpha_A = 5.48, \beta_A = 1.82$ $\gamma_A = 2.00, \tau_{cr} = 3.01$	Stability /(instability) for $\tau < \tau_{cr}/(\tau > \tau_{cr})$

Table 6: Stability of the two BPs case using Amari stability analysis with parameter set A in the Table 1.

analysis for a one-population neural-field model with spatially dependent external drive.

Moreover, in Appendix C we prove that the coefficient $\gamma'_L = 0$ for no or constant external inputs from which it follows that $\lambda = 0$, consistent with the fact that we have translational invariance in that case. This result is in accordance with the result obtained in [24]. However, in the case of spatially dependent external inputs, we find that $\gamma'_L \neq 0$. This is indeed to be expected as this type of inputs represents a symmetry breaking effect in the model.

Let $\tau_{cr}^L \equiv \alpha_L/|\beta_L|$ and $\tau_{cr}^A \equiv \alpha_A/|\beta_A|$ be the critical relative inhibition times obtained by full stability analysis and the Amari analysis, respectively. From the above result we find that $\tau_{cr}^{(L)} > \tau_{cr}^{(A)}$ if the inhibitory external input function $h_i(x)$ is a decreasing function of x. Thus, the Amari analysis predicts conversion to a breather for lower values of the critical inhibition time than the full stability analysis.

Notice that the discrepancy between the full-stability analysis and the Amari analysis is expected to be more pronounced for strongly localized inhibitory external inputs.

We illustrate this feature in the following example using the parameter set A in the Table 1. According to the Amari approach (2), we find that the narrow pulse pair is stable, if the relative inhibition time τ is less than $\tau_{cr} = 0.258$. and becomes unstable if the relative inhibition time exceeds this value of τ_{cr}. The broad pulse pair reveals the same behavior as the narrow pulse pair but with a different critical time constant. It is stable if the relative inhibition time τ is less than $\tau_{cr} = 3.01$ and becomes unstable if $\tau > \tau_{cr}$. In short, the Amari stability analysis predicts both the narrow and broad BP to be stable for sufficiently small relative inhibition time with strongly localized external inputs. In contrast the full stability analysis, cf. Table 5, reveals

Pulse width coordinates	Stability parameters	Stability results
$(a_1, b_1) = (0.112, 0.116)$	$\alpha_L = 2.25, \alpha'_L = 1.07$ $\beta_L = 1.892, \beta'_L = -0.412$ $\gamma_L = -1.029, \gamma'_L = 0.467$ $\tau_{cr} = 1.187, \tau'_{cr} = 2.600$	Saddle point instability
$(a_2, b_2) = (0.180, 0.183)$	$\alpha_L = 5.524, \alpha'_L = 1.632$ $\beta_L = 1.823, \beta'_L = 0.363$ $\gamma_L = 1.927, \gamma'_L = 0.009$ $\tau_{cr} = 3.030, \tau'_{cr} = 4.490$	Stability /(instability) for $\tau < \tau_{cr}/(\tau > \tau_{cr})$

Table 7: Stability results for a two BPs case using full stability analysis with parameters set A in Table 1.

that the narrow BP (a_1, b_1) is unstable for all inhibition time constants τ, because $\gamma'_L < 0$ (see Table 7). The weakness of Amari approach is confirmed numerically by Fig 13. For the broad BP corresponding to the pulse width coordinates (a_2, b_2), we find that $\beta_L > 0$ and $\beta'_L > 0$. Thus, we are in the regime where we have two critical relative inhibition times τ_{cr} and τ'_{cr} (see Table 3 and Table 4). As $\tau_{cr} < \tau'_{cr}$, the broad BP becomes unstable if τ exceeds $\tau_{cr} = 3.03$ (see Table 5). The example also illustrates that the Amari approach yields the wrong stability predictions. Here we will like to point out that the weakness of the Amari approach is confirmed numerically by Fig. 13.

As the Amari analysis fails to predict the correct stability result, we therefore use the full stability analysis for the cases with three and four BPs. The corresponding parameters for three and four BPs case are given by set B and C in Table 1, respectively.

For the three BPs example (Table 8) we find that $\beta_L > 0$ and $\beta'_L < 0$. Therefore, according to the stability theory elaborated in the previous section, the pulse pair corresponding to the intersection (a_1, b_1) in Fig. 7a is unstable if the relative inhibition time τ exceeds $\tau_{cr} = 5.761$.

The second BP corresponding to the point (a_2, b_2) is unstable for all τ, since $\gamma_L < 0$.

For the third pulse pair corresponding to (a_3, b_3), we obtain $\beta_L > 0$ and $\beta'_L > 0$. We notice that $\tau_{cr} < \tau'_{cr}$. Thus the bumps become unstable $\tau > \tau_{cr}$. In short, the narrowest bumps corresponding to (a_1, b_1) and the broadest

Pulse width coordinates	Stability parameters	Stability results
$(a_1, b_1) = (0.080, 0.096)$	$\alpha_L = 1.531, \alpha'_L = 1.020$ $\beta_L = 0.265, \beta'_L = -0.868$ $\gamma_L = 0.174, \gamma'_L = 0.889$ $\tau_{cr} = 5.761, \tau'_{cr} = 1.175$	Stability /(instability) for $\tau < \tau_{cr}/(\tau > \tau_{cr})$ $\tau_{cr} = 5.761$
$(a_2, b_2) = (0.100, 0.107)$	$\alpha_L = 1.861, \alpha'_L = 1.041$ $\beta_L = 0.918, \beta'_L = -0.688$ $\gamma_L = -0.259, \gamma'_L = 0.724$ $\tau_{cr} = 2.016, \tau'_{cr} = 1.512$	Saddle point instability
$(a_3, b_3) = (0.180, 0.183)$	$\alpha_L = 5.525, \alpha'_L = 1.632$ $\beta_L = 1.815, \beta'_L = 0.359$ $\gamma_L = 1.938, \gamma'_L = 0.014$ $\tau_{cr} = 3.045, \tau'_{cr} = 4.546$	Stability /(instability) for $\tau < \tau_{cr}/(\tau > \tau_{cr})$ $\tau_{cr} = 3.045$

Table 8: Stability results for three BPs situation using full stability analysis with the parameter set B in Table 1.

bumps corresponding to (a_3, b_3) are stable for sufficiently small inhibition times, while the bump pair corresponding to the intermediate coordinates (a_2, b_2) is always unstable for the parameters set B in Table 1.

For the example of four BPs solutions, we use the parameters set C in Table 1. Their stability properties are summarized in Table 9. The BPs corresponding to the pulse width coordinates (a_1, b_1) and (a_3, b_3) are always unstable, whereas BPs corresponding to (a_2, b_2) and (a_4, b_4) are stable for small for small and moderate values of the relative inhibition times $\tau < \tau_{cr}$.

Fig. 11 provides an overview of the number of stable BPs (color coded). The computations underlying this plot is based on the stability classification scheme developed in section 5.2. Depending on the input amplitude A_e and A_i, we observe up to three coexisting stable bump-pair solutions.

6. Numerical simulations

In this section we solve the initial value problem (2) numerically by means of the numerical code developed in Appendix B with single bump (19) as initial condition. The connectivity functions and the external input functions are given as gaussians (5), (6) and (7), respectively. The input parameters used here are given by set A in Table 1 and hence the pulse width coordinates

Pulse width coordinates	Stability parameters	Stability results
$(a_1, b_1) = (0.014, 0.072)$	$\alpha_L = 1.243, \alpha'_L = 1.005$ $\beta_L = 1.293, \beta'_L = -0.992$ $\gamma_L = -1.147, \gamma'_L = 0.998$ $\tau_{cr} = 0.961, \tau'_{cr} = 1.013$	Saddle point instability
$(a_2, b_2) = (0.057, 0.086)$	$\alpha_L = 1.367, \alpha'_L = 1.011$ $\beta_L = 0.068, \beta'_L = -0.943$ $\gamma_L = 0.239, \gamma'_L = 0.955$ $\tau_{cr} = 20.12, \tau'_{cr} = 1.072$	Stability /(instability) for $\tau < \tau_{cr}/(\tau > \tau_{cr})$ $\tau_{cr} = 20.12$
$(a_3, b_3) = (0.108, 0.113)$	$\alpha_L = 2.079, \alpha'_L = 1.057$ $\beta_L = 1.464, \beta'_L = -0.535$ $\gamma_L = -0.679, \gamma'_L = 0.583$ $\tau_{cr} = 1.442, \tau'_{cr} = 1.975$	Saddle point instability
$(a_4, b_4) = (0.180, 0.183)$	$\alpha_L = 5.525, \alpha'_L = 1.632$ $\beta_L = 1.819, \beta'_L = 0.361$ $\gamma_L = 1.933, \gamma'_L = 0.011$ $\tau_{cr} = 3.037, \tau'_{cr} = 4.518$	Stability /(instability) for $\tau < \tau_{cr}/(\tau > \tau_{cr})$ $\tau_{cr} = 3.037$

Table 9: Stability results for four BPs using full stability analysis with the parameter set C in Table 1.

of the initial condition are given by (36). Fig. 12 shows the outcome of the numerical simulations of the system (2) with a broad BP as the initial condition with a small perturbation $\epsilon > 0$. i.e. $(a_{eq} + \epsilon,\ b_{eq} + \epsilon)$. For $\tau < \tau_l$ ($\tau_l \approx 2.99$), we observe that both the excitatory and inhibitory pulses are stable (Fig. 12a), whereas for τ in the interval $\tau_l < \tau < \tau_u$ ($\tau_u \approx 3.126$) the pulses behave like stable breathers (Fig. 12b). For $\tau > \tau_u$, the bumps are unstable (Fig. 12c). Notice that the full stability analysis of section 5.2 in this case predicts a change from stability to instability through a breather type of state for $\tau = \tau_{cr} = 3.03$, which is in the interval for the breathers detected by means of the numerical simulations. Hence we can conclude that there is an excellent agreement between the outcome of the numerical simulations and the predictions obtained from the stability analysis for the broad bumps pair. We observe, however, that the critical relative inhibition time predicted by the Amari analysis in this case ($\tau_{cr} = 3.01$) also belongs to the numerically detected interval $\tau_l < \tau < \tau_u$ for breathers. We expect that the discrepancy between these two approaches will show up for broad bumps

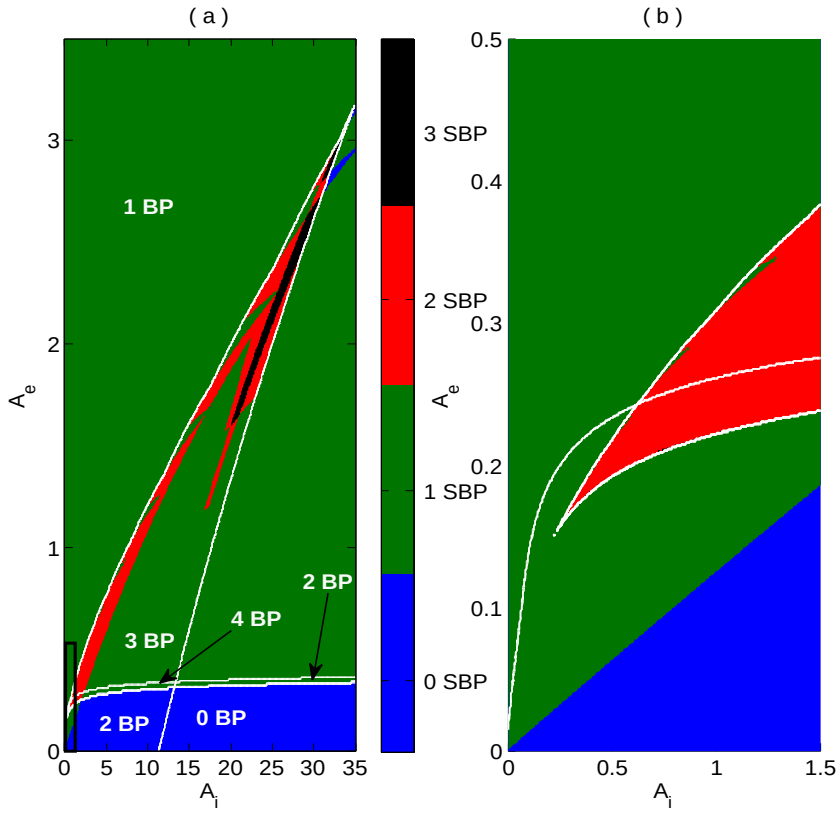

Figure 11: **(a)** Dependence of the number of stable bump pairs (color coded) on the input amplitudes A_e and A_i. Regions with different numbers of solutions are separated by white curves (see Fig. 6). **(b)** Magnified view of the region marked by black rectangle in (a). See Table 1 for parameters.

pair which are even more strongly localized than the bumps pair we use as initial condition in the present numerical study. In the nonlinear stage of the instability the pulse evolution saturates in accordance with the estimates for the bounds (14). This feature is demonstrated in the Fig. 2.

Another notable feature is that for τ exceeding τ_{cr}, we observe that the broad inhibitory bump develops into a new state after the initial linear stage

of the instability, while the excitatory bumps collapse and vanish. This feature has no counterpart in the non-external input case observed in [24]. Hence we conclude that it is an effect of the spatially localization of the external input.

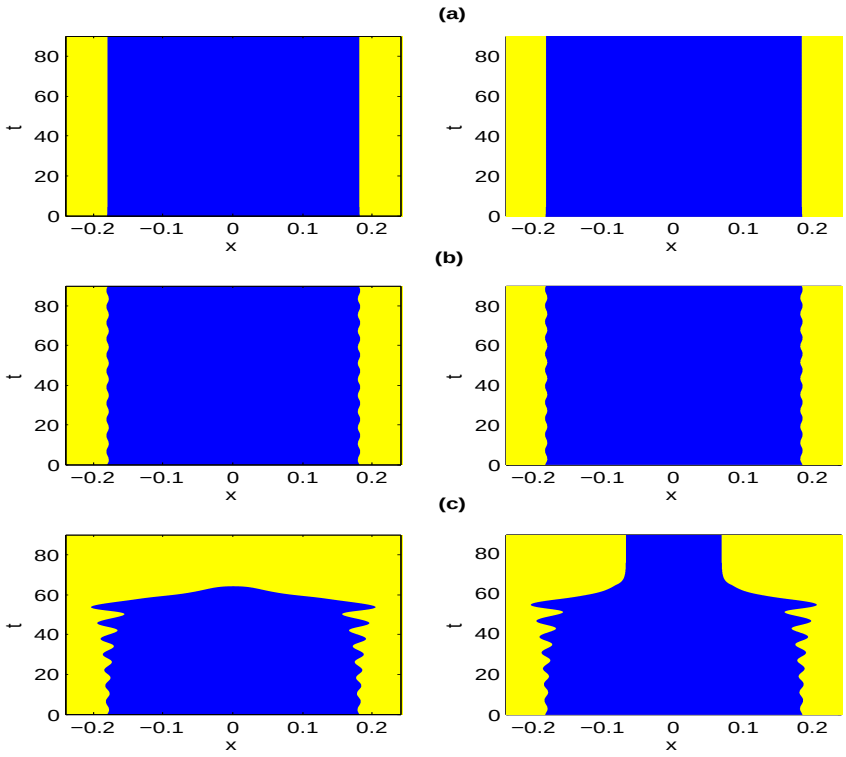

Figure 12: Time evolution of excitatory (left column) and inhibitory firing rates (right column) for a broad bump pair subject to a small perturbation $\epsilon = 0.001$ at time $t = 0$. **(a)** Stable BP ($\tau = 0.24 < \tau_{cr}$). **(b)** Stable breathers ($\tau = \tau_{cr} = 3.03$). **(c)** Unstable BP ($\tau = 3.127 > \tau_{cr}$). Input parameters: Parameter set A in Table 1).

Next, we consider the time evolution of a narrow pulse pair (Fig. 13). For the case of spatially dependent external input the narrow BPs are unstable

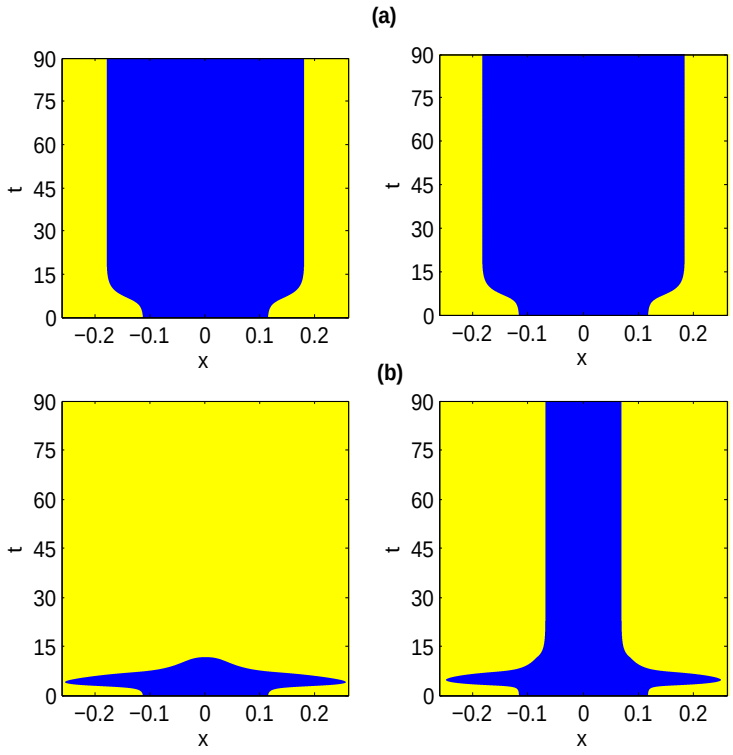

Figure 13: Time evolution of excitatory (left column) and inhibitory firing rates (right column) for a narrow bump pair subject to a small perturbation $\epsilon = 0.001$ at time $t = 0$. **(a)** Unstable narrow BP converts to a stable broad BP ($\tau = 0.24 < \tau_{cr}$). **(b)** Unstable narrow BP converts to a non-BP state with vanishing excitatory and finite bump-like inhibitory firing rate ($\tau = \tau_{cr} = 3.127$). The input parameters: Parameter set A in Table 1).

for all values of τ and is converted to a broad BP for $\tau = 0.24$ (Fig. 12a and Fig. 13a). Also in this case we have excellent agreement between the outcome of the numerical simulations and the stability analysis in the initial stage of the evolution. The Amari analysis predicts that the narrow BP is stable for $\tau \lesssim 0.258$. Fig. 13a demonstrates that the narrow BP is unstable and is converted to broad BP at $\tau = 0.24$. This result also confirms numerically that the Amari approach for stability does not give the right answer regarding

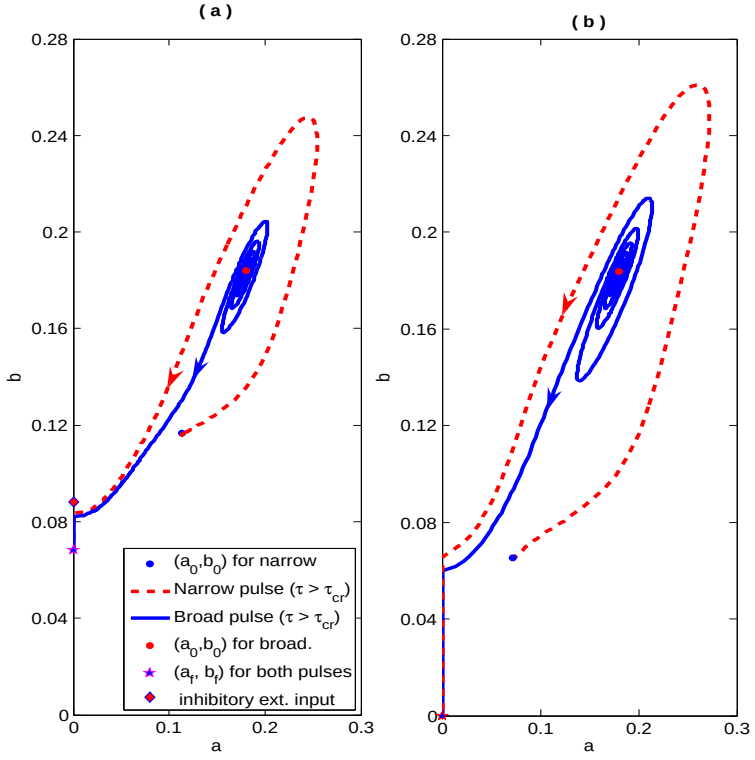

Figure 14: Time evolution $(a(t), b(t))$ of BPs in the pulse-width plane following a small perturbation of a broad (blue solid lines) and a narrow (red dashed lines) stationary bump solution (a_0, b_0) (red and blue dots, respectively). **(a)** Strong input ($A_e = 0.19$, $A_i = 0.7$). **(b)** Weak input ($A_e = 0.075$, $A_i = 0.07$). Asterisks mark final states. Red diamond in (a) represents pulse width of external input targeting the inhibitory population. Time constant $\tau = 3.127 > \tau_{cr}$. All other parameters are as in Fig. 12.

the stability of the bumps. After the initial stage of the instability, we also notice that the narrow inhibitory BPs are converted to new stable states for all τ-values in a way similar to what we have observed for the broad inhibitory bumps in the parameter regime $\tau > \tau_{cr}$, except for small values of τ the excitatory bumps collapse and vanish. Also in this case the nonlinear stage of the instability the pulse evolution saturates in accordance with the estimates for the bounds (14). This feature is demonstrated in the Fig. 2.

In order to understand the formation of the stable inhibitory stationary state we first study the bumps evolution in the pulse width coordinate plane.

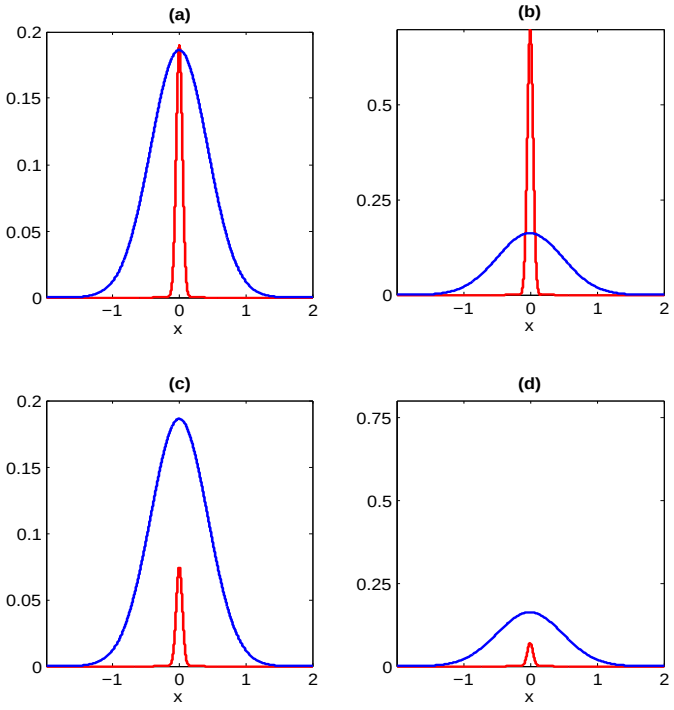

Figure 15: Competition between external input and inhibitory activity in single-bump states with vanishing excitatory activity. Effect of an inhibitory pulse (with pulse width coordinate $b = 0.1$; blue curves) and external input (red curves) on the excitatory (left column; eq. (63a)) and inhibitory population (right column; eq. (63b)) for **(a,b)** strong ($A_e = 0.19$, $A_i = 0.7$) and **(c,d)** weak external input ($A_e = 0.075$, $A_i = 0.07$). The other parameters are as in Table 1.

Fig. 14(a) shows the evolution of pulse width coordinates of narrow (dashed curves) and broad (solid curve) at $\tau = 3.127 > \tau_{cr}$ with parameters given by set A in Table 1. Fig. 14(b) shows the evolution of the pulse width coordinates of the narrow and broad BPs for $\tau > \tau_{cr}$ with smaller amplitude than the threshold values. Notice that the corresponding pulse width coordinates in Fig. 14(a) approach the state $(a, b) = (0, 0.068)$, which corresponds to the stable localized inhibitory stationary state. But if we reduce the amplitudes of the external inputs Fig. 14(b), then both pulse width coordinates tend to zero, which means that no stable localized stationary state is formed.

The formation of the stable inhibitory stationary state in the nonlinear stage of the instability can easily be understood by estimating the order of magnitude of the terms on the right hands side of the model (2) in the actual parameter regime. When considering the model (2) the excitatory effects are very small compared to the inhibitory effects in this stage of the pulse evolution. We hence neglect the excitatory terms in the model and get

$$\frac{\partial}{\partial t}u_e(x,t) = -u_e(x,t) - (W_{ie}(b(t)+x) + W_{ie}(b(t)-x)) + h_e(x) \qquad (63a)$$

$$\tau\frac{\partial}{\partial t}u_i(x,t) = -u_i(x,t) - (W_{ii}(b(t)+x) + W_{ii}(b(t)-x)) + h_i(x) \qquad (63b)$$

as an approximative description of the bumps evolution. Here $W_{im},\ m \in \{e,i\}$ is the antiderivative of ω_{im} defined by (20) and $b(t)$ the time-dependent pulse width coordinate given by the threshold value condition $u_i(b(t),t) = \theta_i$.

The inhibitory effects in the excitatory equation (63a) (modeled by means of the function $W_{ie}(b(t)+x) + W_{ie}(b(t)-x))$) balance the external input (modeled by means of the function $h_e(x)$) in the core of the input i.e in the neighborhood of $x = 0$ when $0.06 \lesssim b \lesssim 0.1$ Outside this region the input effect function $h_e(x)$ is negligible. This feature is demonstrated in Fig. 15. Due to the presence of the linear decay term $-u_e(x,t)$ we then get a decay of the excitatory activity level and hence no new excitatory stationary stable can be formed. In the inhibitory equation (63b), however, the external input function $h_i(x))$ in the vicinity of $x = 0$ is much larger than the function $W_{ii}(b(t)+x) + W_{ii}(b(t)-x)$ modeling the inhibitory effects and negligible outside this region for the actual parameter regime. See Fig. 15. Hence the external input in (63b) can balance the natural linear decay term $-u_i(x,t)$ and the inhibitory effects. The outcome of this balance is a new localized inhibitory stationary state, which is strongly localized and has almost the same shape as the input function $h_i(x)$. If we reduce the amplitude parameter in the inhibitory input function $h_i(x)$ so that this input becomes of the order of magnitude of the inhibitory effects function $W_{ii}(b(t)+x)+W_{ii}(b(t)-x)$ in the core of the input, no such balance is possible any more, and hence new stable states will not be formed in that case.

7. Conclusions

In this paper we have studied the extension of the model studied by Blomquist et al [24] by including spatially dependent external input.

The solutions of the initial value problem (2) are bounded for finite external input. The existence of localized stationary symmetric solutions (BP) of the model (2) has been investigated as a function of the amplitude of localized external input function. Stability of these BPs has been investigated by using Amari approach and full stability analysis. The Amari stability analysis fails to give correct stability predictions. We have detected at most four BPs with maximum three stable BPs.

Bounded solutions of the initial value problem (2) depicts that any instability detected has to be saturated. It is shown that the bumps exist for small and moderate values of the external input amplitudes. In the regime of large amplitudes of the external inputs we have no bumps. Notice that this should be compared with the situation without external inputs treated in Blomquist et al [24] where we always have an admissible set of threshold values i.e. we can always find threshold values producing bumps.

We have identified the number of bumps as a function of different input parameters: The threshold value plane and the external amplitude plane. In the regime of wide external inputs we get a situation which is very much alike to what we have in the zero input case. The common picture consists of two bumps pair for a given pair of admissible threshold values, one narrow bumps pair and one broad bumps pair. This is to be expected as the wide external inputs case can be considered as a perturbation of the no input case. In the complementary regime i.e. when we have a strongly localized external inputs we can identify regimes of the input parameters (= threshold values and external amplitude parameters) corresponding to three and four bumps pairs. This is a completely new feature which has no counterpart in the non-input/wide input case. To our knowledge this feature has not been observed earlier.

We then show that the outcome of the simplified stability analysis of the Amari type disagrees with the predictions obtained from full stability analysis: In the full stability analysis we get a 4×4 stability matrix (Evans matrix) which can be block-diagonalized. The upper block corresponds to the spatial symmetric part of the perturbations, the lower block to the anti-symmetric perturbations. However, as opposed to the results in Blomquist et al [24], the upper block in this case does not produce the same growth rate equation as the Amari approach, and the translational invariance of the bumps is not recovered from the lower block. This is caused by the spatial localization of the external inputs. Observe that this result is qualitatively different from the one observed for bumps in a one-population model with

spatially dependent external drive [19] where it is found that the Amari approach and the full stability analysis agree. The full stability analysis divides the bumps pairs into two groups in the same way as in Blomquist et al [24]: One group of bumps pairs is unstable for all relative inhibition times (saddle point instability). The narrow bumps pairs typically belong to this group. The second group is characterized by bumps pairs which are stable for small and moderate values of the relative inhibition time and which are converted to unstable states through a breather type of state as the relative inhibition time exceeds a certain threshold value. The Amari analysis also predicts the existence of a critical threshold value of the relative inhibition time for which bumps are converted from stable to unstable states through a breather type of state. However, for inhibitory external inputs modeled by means of functions which are decreasing for positive argument, it is shown that the critical relative inhibition time predicted by the Amari approach is less than the one predicted by full stability analysis. The discrepancy typically shows up in the case of strongly localized inhibitory external inputs. This result is completely different from the result obtained by Folias et al [19] for a one-population model with spatially dependent external input, where the stability analysis based on the Amari approach agrees with the full stability analysis.

We demonstrate the discrepancy between predictions obtained from the Amari analysis and the full stability analysis in a concrete striking example consisting of a two bump-pairs. The Amari analysis yields stability for both bump pairs, while the full stability analysis predicts that first bump pair (the narrow one) to be unstable for all relative inhibition times, while the second (broad) bump pair is stable for small and moderate values of the relative inhibition times. We also investigate the stability of the bumps in a three and a four bump-pair situations. For the three bump-pair case which we have studied, the bumps corresponding to the smallest and largest pulse width coordinates are stable for small and moderate values of the relative inhibition times, while the middle pulse width case yields unstable bumps for all relative inhibition times. In the four-bumps case, we have two stable bumps pair for small and moderate values of the relative inhibition times and two bumps pair which are unstable for all relative inhibition times. It is an important feature in the neuroscience to have a system which produces several coexisting stable BPs. Each bump pair could represent a pattern to be stored and also bump state represent a persistent short term memory [7]. The more stable bumps depicts more memory capacity of the network

[34, 35].

Finally, we compare the predictions obtained from the full stability analysis with the outcome of the numerical simulations where we use a bumps pair in the strongly localized regime as initial conditions. The simulations are based on fourth order Runge Kutta method in time and is a slight modification of the code developed in Blomquist et al [24]. We get excellent agreement between numerical results and analytical predictions. Moreover, we show that the nonlinear stage of the instability of both the broad and narrow inhibitory bumps consist of a stable localized inhibitory bumps. The excitatory bumps collapse and vanish in this stage of the pulse evolution.

In the present paper we have approximated the firing rate functions with Heaviside functions. We conjecture that the model (2) with this simplification reproduces qualitatively the same features as the model (2) with sigmoidal firing rate functions. While this conjecture is supported by numerical simulations (see for example [25]), there are few and far between the works addressing this problem in a rigorous mathematical way. We believe, however, that this problem can be dealt with methods of nonlinear functional analysis and degree theory in a way analogous to Oleynik et al [36] and singular perturbation analysis in a similar way as in Yousaf et al [37]. We do not pursue this problem here, however, but will return to it in future investigations.

Acknowledgements

The authors would like to thank Professor Arkadi Ponossov and Dr. Hans Ekkehard Plesser (Norwegian University of Life Sciences) and Professor Stephen Coombes (The University of Nottingham, UK) for many fruitful and stimulating discussions during the preparation of this paper. This research was supported by the Norwegian University of Life Sciences. The work has also been supported by The Research Council of Norway under the grant No. 178892 (eNEURO-multilevel modeling and simulation of the nervous system). Muhammad Yousaf would like to thank the Higher Education Commission of Pakistan for support. The authors will also like to thank the reviewers for constructive remarks.

Appendix A. Derivation of characteristic equations in the full stability analysis

Using (54), the system (53) becomes

$$(\lambda+1)\kappa_1(x) = \omega_{ee} \otimes \delta((U_e-\theta_e)\kappa_1) - \omega_{ie} \otimes \delta((U_i-\theta_i)\chi_1) \tag{A.1a}$$

$$(\tau\lambda+1)\chi_1(x) = \omega_{ei} \otimes \delta((U_e-\theta_e)\kappa_1) - \omega_{ii} \otimes \delta((U_i-\theta_i)\chi_1) \tag{A.1b}$$

We now assume that there is one-to-one correspondence between the pulse width coordinates (a_{eq}, b_{eq}) and the bumps $(U_e(x), U_i(x))$ through the relation

$$U_e(a_{eq}) = \theta_e \ \ , \ \ U_i(b_{eq}) = \theta_i \tag{A.2}$$

The convolution integrals of the type $\omega \otimes \delta((U-\theta)\kappa)$ are according to [8, 24] given as

$$\omega \otimes \delta((U-\theta)\kappa) = \frac{1}{|U'(a)|}[\omega(x+a)\kappa(-a) + \omega(x-a)\kappa(a)]$$

with $U(\pm a) = \theta$. We hence end up with the system

$$\begin{aligned}(\lambda+1)\kappa_1(x) = &\frac{1}{|U_e'(a_{eq})|}[\omega_{ee}(x+a_{eq})\kappa_1(-a_{eq}) + \omega_{ee}(x-a_{eq})\kappa_1(a_{eq})] \\ &- \frac{1}{|U_i'(b_{eq})|}[\omega_{ie}(x+b_{eq})\chi_1(-b_{eq}) + \omega_{ie}(x-b_{eq})\chi_1(b_{eq})]\end{aligned} \tag{A.3a}$$

$$\begin{aligned}(\lambda\tau+1)\chi_1(x) = &\frac{1}{|U_e'(a_{eq})|}[\omega_{ei}(x+a_{eq})\kappa_1(-a_{eq}) + \omega_{ei}(x-a_{eq})\kappa_1(a_{eq})] \\ &- \frac{1}{|U_i'(b_{eq})|}[\omega_{ii}(x+b_{eq})\chi_1(-b_{eq}) + \omega_{ii}(x-b_{eq})\chi_1(b_{eq})]\end{aligned} \tag{A.3b}$$

Since $U_e'(a_{eq})$ and $U_i'(b_{eq})$ by assumption are negative, we have

$$|U_e'(a_{eq})| = \omega_{ee}(0) - \omega_{ee}(2a_{eq}) + \omega_{ie}(a_{eq}+b_{eq}) - \omega_{ie}(a_{eq}-b_{eq}) - h_e'(a_{eq}) \tag{A.4}$$

and

$$|U_i'(b_{eq})| = \omega_{ei}(b_{eq}-a_{eq}) - \omega_{ei}(a_{eq}+b_{eq}) + \omega_{ii}(2b_{eq}) - \omega_{ii}(0) - h_i'(b_{eq}) \tag{A.5}$$

The system equations (A.3) imply the equivalence

$$\left.\begin{aligned} &\kappa_1(a_{eq}) = \kappa_1(-a_{eq}) = \chi_1(b_{eq}) = \chi_1(-b_{eq}) \equiv 0 \\ &\Leftrightarrow \kappa_1(x) = \ \chi_1(x) \equiv 0 \end{aligned}\right\} \tag{A.6}$$

Since we are looking for non-trivial spatial perturbations, we must assume that

$$\underline{X} = \begin{bmatrix} \kappa_1(a_{eq}) \\ \kappa_1(-a_{eq}) \\ \chi_1(b_{eq}) \\ \chi_1(-b_{eq}) \end{bmatrix} \neq \underline{0} \tag{A.7}$$

The problem consists of finding the λ for which (A.7) holds true. Let $x = \pm a_{eq}$ and $x = \pm b_{eq}$ in (A.3). We get the system of four linear homogenous equations in four unknowns $\kappa_1(a_{eq})$, $\kappa_1(-a_{eq})$, $\chi_1(b_{eq})$ and $\chi_1(-b_{eq})$, which can be expressed in the matrix form as

$$\mathbf{A} \cdot \underline{\mathbf{X}} = \underline{\mathbf{O}} \tag{A.8}$$

Here $\underline{\mathbf{X}}$ is defined by (A.7), while the matrix $\mathbf{A}$ is given as

$$\mathbf{A} = \begin{bmatrix} A_1 - (\lambda+1) & A_2 & -A_3 & -A_4 \\ A_2 & A_1 - (\lambda+1) & -A_4 & -A_3 \\ C_1 & C_2 & -C_3 - (\lambda\tau+1) & -C_4 \\ C_2 & C_1 & -C_4 & -C_3 - (\lambda\tau+1) \end{bmatrix} \tag{A.9}$$

where A_s and C_s for $s = 1,\ 2,\ 3,\ 4$ are given by (59). Now, consider the matrix $\mathbf{P}$

$$\mathbf{P} = \begin{bmatrix} \frac{1}{2} & \frac{1}{2} & 0 & 0 \\ 0 & 0 & \frac{1}{2} & \frac{1}{2} \\ \frac{1}{2} & -\frac{1}{2} & 0 & 0 \\ 0 & 0 & \frac{1}{2} & -\frac{1}{2} \end{bmatrix} \tag{A.10}$$

and introduce the substitution

$$\underline{\mathbf{Y}} = \mathbf{P} \cdot \underline{\mathbf{X}} \tag{A.11}$$

We readily find that

$$\underline{\mathbf{Y}} = \begin{bmatrix} \frac{1}{2}\{\kappa_1(a_{eq}) + \kappa_1(-a_{eq})\} \\ \frac{1}{2}\{\chi_1(b_{eq}) + \chi_1(-b_{eq})\} \\ \frac{1}{2}\{\kappa_1(a_{eq}) - \kappa_1(-a_{eq}) \\ \frac{1}{2}\{\chi_1(b_{eq}) - \chi_1(-b_{eq})\} \end{bmatrix} = \begin{bmatrix} \kappa_e(a_{eq}) \\ \chi_e(b_{eq}) \\ \kappa_o(a_{eq}) \\ \chi_o(b_{eq}) \end{bmatrix} \tag{A.12}$$

Here $\underline{\mathbf{Y}}$ is the vector containing the even and odd parts of κ_1 and χ_1 evaluated at a_{eq} and b_{eq}. Here the subscripts "e" and "o" stand for even and odd terms, respectively. The similarity transformation from (A.8) to (A.11) transforms the matrix $\mathbf{A}$ to the block diagonal matrix $\mathbf{PAP}^{-1}$, which can be written in a simplified form as

$$\mathbf{PAP}^{-1} = \begin{bmatrix} \mathbf{M}_1 & O \\ O & \mathbf{M}_2 \end{bmatrix} \tag{A.13}$$

where $\mathbf{M}_1$ and $\mathbf{M}_2$ are given as

$$\mathbf{M}_1 = \begin{bmatrix} A_1 + A_2 - \lambda - 1 & -A_3 - A_4 \\ \\ C_1 + C_2 & -C_3 - C_4 - \lambda\tau - 1 \end{bmatrix} \tag{A.14}$$

$$\mathbf{M}_2 = \begin{bmatrix} A_1 - A_2 - \lambda - 1 & -A_3 + A_4 \\ \\ C_1 - C_2 & -C_3 + C_4 - \lambda\tau - 1 \end{bmatrix} \tag{A.15}$$

The determinant of $\mathbf{M}_1$ is

$$|\mathbf{M}_1| = \tau\lambda^2 + (\alpha_L - \beta_L\tau)\lambda + \gamma_L \tag{A.16}$$

Similarly, the determinant of $\mathbf{M}_2$ can be calculated as

$$|\mathbf{M}_2| = \tau\lambda^2 + (\alpha'_L - \beta'_L\tau)\lambda + \gamma'_L \tag{A.17}$$

Hence the determinant of a block diagonal matrix $\mathbf{PAP}^{-1}$ factorizes as

$$\det(\mathbf{PAP}^{-1}) = (\tau\lambda^2 + (\alpha_L - \beta_L\tau)\lambda + \gamma_L) \cdot (\tau\lambda^2 + (\alpha'_L - \beta'_L\tau)\lambda + \gamma'_L) \tag{A.18}$$

The condition for having nontrivial perturbations leads to $\det(\mathbf{PAP}^{-1}) = 0$ from which the characteristic equations (55) and (58) follow.

Appendix B. Runge-Kutta split step method

In this section we will use the Runge-Kutta method to develop a scheme to solve the initial value problem of (2). In this scheme the firing rate functions are approximated with the Heaviside function. The numerical code is given by the code worked out in Blomquist et al [24] extended with external input terms. For the sake of completeness we review it here.

We introduce a finite time sequence t_j (with j=0,1,2,3...). Here each time t_j represents specific time of observation with $t_0 = 0$ and time stepping length is $\triangle t_j = t_{j+1} - t_j$. For each time step we will observe both $(u_e(x,t_j), u_i(x,t_j))$ and $(a(t_j), b(t_j))$. We design a numerical code for the two population model for given initial condition. Let $\underline{X}_j$ and $\underline{F}(X)$ be the vector fields defined as

$$\underline{X}_j = \begin{pmatrix} u_e(x,t_j) \\ u_i(x,t_j) \end{pmatrix}, \ \underline{F}(\underline{X}_j) = \begin{pmatrix} f_j \\ g_j \end{pmatrix} \tag{B.1}$$

where f_j and g_j are given as

$$f_j = -u_e + \frac{1}{\tau}\Phi_j \tag{B.2}$$

$$g_j = \frac{1}{\tau}[-u_i + \Psi_j] \tag{B.3}$$

with Φ_j and Ψ_j are given as

$$\begin{aligned} \Phi_j(x) =& W_{ee}(a(t_j)+x) + W_{ee}(a(t_j)-x) \\ &+ W_{ie}(b(t_j)+x) - W_{ie}(b(t_j)-x) + h_e(x) \end{aligned} \tag{B.4a}$$

$$\begin{aligned} \Psi_j(x) =& W_{ei}(a(t_j)+x) + W_{ei}(a(t_j)-x) \\ &+ W_{ii}(b(t_j)+x) - W_{ii}(b(t_j)-x) + h_i(x) \end{aligned} \tag{B.4b}$$

where W_{mn} is the anti-derivative of ω_{mn} defined by means of (20). The pulse width coordinates $a(t_j)$, $b(t_j)$ of excitatory and inhibitory pulses satisfy

$$u_e(a(t_j), t_j) = \theta_e \ , \qquad u_i(b(t_j), t_j) = \theta_i \tag{B.5}$$

The fourth order Runge-Kutta method is divided into two steps. First, we evaluate the slopes $\underline{k}_1, \underline{k}_2, \underline{k}_3, \underline{k}_4$ using $\underline{F}(\underline{X}_j)$

$$\underline{k}_1 = \Delta t_j \cdot \underline{F}(\underline{X}_j) \tag{B.6a}$$

$$\underline{k}_2 = \Delta t_j \cdot \underline{F}(\underline{X}_j + \frac{1}{2}\underline{k}_1) \tag{B.6b}$$

$$\underline{k}_3 = \Delta t_j \cdot \underline{F}(\underline{X}_j + \frac{1}{2}\underline{k}_2) \tag{B.6c}$$

$$\underline{k}_4 = \Delta t_j \cdot \underline{F}(\underline{X}_j + \underline{k}_3) \tag{B.6d}$$

In second step, the next iterated value for $\underline{X}_{j+1}$ is calculated as

$$\underline{X}_{j+1} = \underline{X}_j + \frac{1}{6}(\underline{k}_1 + 2\,\underline{k}_2 + \,2\,\underline{k}_3 + \,\underline{k}_4) \tag{B.7}$$

Formally, the iteration process with initial conditions $(u_e(x,0), u_i(x,0)) = (U_e(x), U_i(x))$ can be explained as follows:

1.) We find the values of the pulse widths $a(0), b(0)$ by solving the system of equations

$$U_e(a(0)) = \theta_e\ , \quad U_i(b(0)) = \theta_i \tag{B.8}$$

By substituting $(a(0), b(0))$ into the equations (B.4a) and (B.4b), we get Φ_0, Ψ_0. Using Φ_0, Ψ_0 we get $\underline{F}_0$. The iterates $u_e(x,t_1), u_i(x,t_1)$ are found by using (B.6) and (B.7).

2.) By following the same procedure we compute the pulse widths coordinates $a(t_1), b(t_1)$ by solving

$$u_e(a(t_1), t_1) = \theta_e\ , \quad u_i(b(t_1), t_1) = \theta_i \tag{B.9}$$

Determine the iterates $u_e(x,t_2), u_i(x,t_2)$ by (B.6) and (B.7). :
:
:

j.) Compute $a(t_{j-1}), b(t_{j-1})$ by solving

$$u_e(a(t_{j-1}), t_{j-1}) = \theta_e\ , \quad u_i(b(t_{j-1}), t_{j-1}) = \theta_i \tag{B.10}$$

Determine the iterates $u_e(x,t_j), u_i(x,t_j)$ by (B.6) and (B.7). Here $(t_j = t_{j-1} + \Delta t_{j-1})$.
:
:
:

The iteration scheme presupposes that there is a one-to-one correspondence between the pulse width coordinates $(a(t), b(t))$ and the threshold values (θ_e, θ_i) for $(a(t) > 0, b(t) > 0)$. Due to the continuous dependence on time t, this property is always fulfilled locally in time if the system $U_e(a(0)) = \theta_e, U_i(b(0)) = \theta_i$ possesses a unique solution.

Appendix C. Proofs of identities used in the stability analysis

Here we will prove the identities

1.) $\alpha_L = \alpha_A - \frac{2h_i'(b_{eq})}{|U_i'(b_{eq})|}$
2.) $\beta_L = \beta_A$
3.) $\gamma_A = \gamma_L - Q, \quad Q \equiv 2\frac{h_i'(b_{eq})}{|U_i'(b_{eq})|}(2A_2 - A_4 + A_3) + 2\frac{h_i'(b_{eq}).h_e'(a_{eq})}{|U_i'(b_{eq})|.|U_e'(a_{eq})|}$
4.) $\gamma_L' \neq 0$

Here α_L, β_L, γ_L, α_A, β_A and γ_A are defined by the equations (57), (45d, 45a) and (47), respectively.

The parameters α_A, β_A, γ_A and α_L, β_L, γ_L depend on the connectivity functions in a complicated way. We conveniently express these parameters in terms of the constants A_s and C_s for $s = 1, 2, 3, 4$ defined by means of (59).

Appendix C.1. $\alpha_L = \alpha_A - \frac{2h_i'(b_{eq})}{|U_i'(b_{eq})|}$

The expressions for α_L and α_A are given as

$$\alpha_L = C_3 + C_4 + 1 = \frac{\omega_{ii}(0)+\omega_{ii}(2b_{eq})+|U_i'(b_{eq})|}{|U_i'(b_{eq})|} \tag{C.1}$$

$$\alpha_A = \frac{1}{|U_i'(b_{eq})|}\{2\,\omega_{ii}(2b_{eq}) - \omega_{ei}(a_{eq}+b_{eq}) + \omega_{ei}(b_{eq}-a_{eq}) + h_i'(b_{eq})\} \tag{C.2}$$

Using (A.5), we can rewrite the expression(C.1) as

$$\alpha_L = \frac{2\omega_{ii}(2b_{eq}) + \omega_{ei}(b_{eq}-a_{eq}) - \omega_{ei}(a_{eq}+b_{eq}) - h_i'(b_{eq})}{|U_i'(b_{eq})|} \tag{C.3}$$

$$= \frac{2\omega_{ii}(2b_{eq}) + \omega_{ei}(b_{eq}-a_{eq}) - \omega_{ei}(a_{eq}+b_{eq}) + h_i'(b_{eq})}{|U_i'(b_{eq})|} - \frac{2h_i'(b_{eq})}{|U_i'(b_{eq})|} \tag{C.4}$$

Now, by comparing (C.2) and (C.4), we get

$$\alpha_L = \alpha_A - \frac{2h_i'(b_{eq})}{|U_i'(b_{eq})|} \tag{C.5}$$

Appendix C.2. $\beta_L = \beta_A$

The expressions for β_L and β_A are given as

$$\beta_L = A_1 + A_2 - 1 = \frac{\omega_{ee}(0) + \omega_{ee}(2a_{eq}) - |U_e'(a_{eq})|}{|U_e'(a_{eq})|} \tag{C.6}$$

$$\beta_A = \frac{1}{|U_e'(a_{eq})|}\{2\,\omega_{ee}(2a_{eq}) - \omega_{ie}(a_{eq}+b) + \omega_{ie}(a_{eq}-b) + h_e'(a_{eq})\} \tag{C.7}$$

By using (A.4), the expression (C.6) can be rewritten as

$$\beta_L = \frac{2\omega_{ee}(2a_{eq}) + \omega_{ie}(a_{eq}-b_{eq}) - \omega_{ie}(a_{eq}+b_{eq}) + h_i'(a_{eq})}{|U_e'(a_{eq})|} \tag{C.8}$$

Then, by comparing (C.7) and (C.8) we get

$$\beta_L = \beta_A \tag{C.9}$$

Appendix C.3. $\gamma_A = \gamma_L - Q$

The expressions for γ_L and γ_A are given as

$$\gamma_L = (C_1 + C_2)(A_3 + A_4) - (C_3 + C_4 + 1)(A_1 + A_2 - 1) \tag{C.10}$$

$$\gamma_A = \mu_A\eta_A - \alpha_A\beta_A \tag{C.11}$$

Then, by simplifying γ_L using (A.4), (A.5) and (59), we obtain

$$\gamma_L = 2A_2C_2 - 4A_2C_4 - 2A_2C_1 + 2A_4C_4 + 2A_4C_1 - 2A_3C_4$$

$$+2A_3C_2 + Q_1(2A_2 - A_4 + A_3) - Q_2(2C_4 - C_2 + C_1) + Q_1Q_2 \tag{C.12}$$

where $Q_1 = \frac{h_i'(b_{eq})}{|U_i'(b_{eq})|}$ and $Q_2 = \frac{h_e'(a_{eq})}{|U_e'(a_{eq})|}$. By using the assumptions (59), the parameters μ_A, η_A, α_A and β_A can be written as

$$\begin{aligned}
\mu_A &= C_2 + C_1 \\
\eta_A &= A_3 + A_4 \\
\alpha_A &= 2C_4 - C_2 + C_1 + Q_1 \\
\beta_A &= 2A_2 - A_4 + A_3 + Q_2
\end{aligned}$$

Hence the expression (C.11) can be written as

$$\gamma_A = 2A_2C_2 - 4A_2C_4 - 2A_2C_1 + 2A_4C_4 + 2A_4C_1 - 2A_3C_4$$

$$+2A_3C_2 - Q_1(2A_2 - A_4 + A_3) - Q_2(2C_4 - C_2 + C_1) - Q_1Q_2 \quad \text{(C.13)}$$

Comparing (C.12) and (C.13) we get

$$\gamma_A \quad = \gamma_L - 2\frac{h_i'(b_{eq})}{|U_i'(b_{eq})|}(2A_2 - A_4 + A_3) - 2\frac{h_i'(b_{eq}).h_e'(a_{eq})}{|U_i'(b_{eq})|.|U_e'(a_{eq})|} \quad \text{(C.14)}$$

Appendix C.4. $\gamma_L' \neq 0$

The expression for γ_L' is given as

$$\gamma_L' = (C_1 - C_2) \cdot (A_3 - A_4) - (C_3 - C_4 + 1)(A_1 - A_2 - 1) \quad \text{(C.15)}$$

Using (59)

$$\gamma_L' = 1 - L_1 + L_2 + L_3 + L_4$$

where

$$L_1 = \frac{\omega_{ee}(2a_{eq}) - \omega_{ee}(0)}{|U_e'(a_{eq})|}, \quad L_2 = \frac{\omega_{ii}(0) - \omega_{ii}(2b_{eq})}{|U_i'(b_{eq})|}$$

$$L_3 = (\frac{\omega_{ee}(2a_{eq}) - \omega_{ee}(0)}{|U_e'(a_{eq})|})(\frac{\omega_{ii}(0) - \omega_{ii}(2a_{eq})}{|U_i'(b_{eq})|})$$

$$L_4 = \left(\frac{\omega_{ie}(a_{eq} - b_{eq}) - \omega_{ie}(a_{eq} + b_{eq})}{|U_e'(a_{eq})|}\right) \cdot \left(\frac{\omega_{ei}(a_{eq} - b_{eq}) - \omega_{ei}(a_{eq} + b_{eq})}{|U_i'(b_{eq})|}\right)$$

Hence (C.15) can be written as

$$\gamma_L' = 1 + \frac{d_2d_3 + d_5d_6}{|U_e'(a_{eq})||U_i'(b_{eq})|} + \frac{d_2}{|U_e'(a_{eq})|} + \frac{d_3}{|U_i'(b_{eq})|} \quad \text{(C.16)}$$

where

$$d_2 = \omega_{ee}(2a_{eq}) - \omega_{ee}(0)\ , \quad d_3 = \omega_{ii}(0) - \omega_{ii}(2b_{eq})$$

$$d_5 = \omega_{ie}(a_{eq} - b_{eq}) - \omega_{ie}(a_{eq} + b_{eq}) \ , \quad d_6 = \omega_{ei}(a_{eq} - b_{eq}) - \omega_{ei}(a_{eq} + b_{eq})$$

Now, by using (A.4) and (A.5)

$$|U_e'(a_{eq})||U_i'(b_{eq})| = d_2 d_3 - d_5 d_6 + d_3 d_5 - d_2 d_6 + Q_3$$

where

$$Q_3 = h_e'(a_{eq})d_3 + h_i'(b_{eq})d_2 - h_e'(a_{eq})d_6 + h_i'(b_{eq})d_5 + h_e'(a_{eq})h_i'(b_{eq})$$

Then by tedious algebraic calculations we end up with following relation

$$\gamma_L' = \frac{h_i'(b_{eq})d_5 - h_e'(a_{eq})d_6 + h_e'(a_{eq})h_i'(b_{eq})}{d_2 d_3 - d_5 d_6 + d_3 d_5 - d_2 d_6 + Q_3} \tag{C.17}$$

Hence $\gamma_L' \neq 0$.

References

[1] Funahashi S, Bruce CJ, Goldman-Rakic PS, Mnemonic coding of visual space in the monkeys dorsolateral prefrontal cortex. J. Neurophysiol. 61 (1989) 31–349.

[2] Goldman-Rakic PS, Cellular basis of working memory, Neuron. 14 (1995) 477–485.

[3] Miller EK, Erickson CA, Desimone R, Neural mechanisms of visual working memory in prefrontal cortex of the macaque, J. Neurosci. 16 (1996) 5154–5167.

[4] Wang XJ, Synaptic basis of cortical persistent activity: the importance of NMDA receptors to working memory, J. Neurosci. 19 (1999) 9587–9603.

[5] Durstweitz D, Seamans JK, Sejnowski TJ, Neurocomputational models of working memory, Nature Neurosci. 3 (2000) 1184–1191.

[6] Compte A, Brunel N, Goldman-Rakic PS, Wang X, Synaptic mechanisms and network dynamics undelying spatial working memory in the cortical network model, Cereb. Cort. 10 (2000) 1627-1647.

[7] Wang XJ, Synaptic reverberation underlying mnemonic persistent activity, Trend Neurosci, 24 (2004) 455–463.

[8] Coombes S, Waves, bumps, and patterns in neural field theories, Biol Cybern. 93 (2005) 91–108.

[9] Amari S, Dynamics of pattern formation in lateral-inhibition type neural fields, Biol Cybern. 27 (1977) 77–87.

[10] Wilson HR, Cowan JD, Excitatory and inhibitory interactions in localized populations of model neurons, Biophys. J. 12 (1972) 1–24.

[11] Wilson HR, Cowan JD, A mathematical theory of the functional dynamics of cortical and thalamic nervous tissue, Kybernetik. 13 (1973) 55–80.

[12] Ermentrout B, Neural networks as spatio-temporal pattern-forming systems, Rep. Prog. Phys. 61 (1998) 353–430.

[13] Wyller J, Blomquist P, Einevoll GT, On the origin and properties of two-population neural field models: A tutorial introduction, Biophys. Reviews Letters. 2 (2007) 79–98.

[14] Kishimoto K, Amari S, Existence and stability of local excitations in homogeneous neural fields, J. Math. Biol. 7 (1979) 303–318.

[15] Pinto DJ, Ermentrout GB, Spatially structured activity in synaptically coupled neuronal networks: II. Lateral inhibition and standing pulses, SIAM J. Appl. Math. 62 (2001) 226–243.

[16] Laing CR, Troy WC, Gutkin B, Ermentrout GB, Multiple bumps in a neuronal model of working memory, SIAM J. Appl. Math. 63 (2002) 62–97.

[17] Coombes C, Lord GJ, Owen MR, Waves and bumps in neuronal networks with axo-dendritic synaptic interactions, Physica D. 178 (2003) 219–241.

[18] Laing CR, Troy WC, Two-bump solutions af Amari-type models of neuronal pattern formation, Physica D. 178 (2003) 190–218.

[19] Folias SE, Bressloff PC, Breathing pulses in an excitatory network, SIAM J. Appl. Dyn. Syst. 3 (2004) 378–407.

[20] Rubin JE, Troy WC, Sustained spatial patterns of activity in neuronal populations without recurrent excitation, SIAM J. Appl. Math. 64 (2004) 1609–1635.

[21] Coombes S, Owen MR, Bumps, breathers, and waves in a neural network with spike frequency adaptation, Phys. Rev. Lett. 2005 148102.

[22] Guo Y, Chow CC, Existence and stability of standing pulses in neural networks: I. Existence, SIAM J. Appl. Dyn. Syst. 4 (2005) 217–248.

[23] Guo Y, Chow CC, Existence and stability of standing pulses in neural networks: II. Stability, SIAM J. Appl. Dyn. Syst.4 (2005) 249–281.

[24] Blomquist P, Wyller J, Einevoll GT, Localized activity patterns in two-population neuronal network, Physica D 206 (2005) 180–212.

[25] Wyller J, Blomquist P, Einevoll GT, Turing instability and pattern formation in a two-population neuronal network model, Physica D. 225 (2007) 75–93.

[26] Kilpatrick ZP, Bressloff PC, Stability of bumps in piecewise smooth neural fields with nonlinear adaptation, Physica D. 239 (2010) 1048–1060.

[27] Oleynik A, Wyller J, Tetzlaff T, Einevoll GT, Stability of bumps in a two-population neural-field model with quasi-power temporal kernels, Nonlinear Analysis: Real World App. 12 (2011) 3073–3094.

[28] Hubel D, Wiesel T, Receptive fields, binocular interaction and functional architecture in the cat's visual cortex, J. Physiol. 160 (1962) 106–154.

[29] Ben-Yishai R, Bar-Or RL, Sompolinsky H, Theory of orientation tuning in visual cortex, Proc. Natl. Acad. Sci. 92 (1995) 3844–3848.

[30] Ferster D, Miller KD, Neural mechanisms of orientation selectivity in the visual cortex, Ann. Rev. Neurosci. 23 (2000) 441–471.

[31] Veltz R, Faugeras O, Stability of the stationary solutions of neural field equations with propagation delays, J. Math. Neurosci. 1 (2011) 1–25.

[32] Potthast R, Graben PB, Existence and properties of solutions for neural field equations, Mathematical Methods in the Applied Sciences (www.interscience.wiley.com). DOI: 10.1002/mma.1199.

[33] Faye G, Faugeras O, Some theoretical and numerical results for delayed neural field equations, Physica D. 239 (2010) 561–578.

[34] Rolls ET, Attractor networks, Wiley Interdisciplinary Reviews: Cognitive Science. 1(2010) 119–134.

[35] Hu X, Zhang B, A Gaussian attractor network for memory and recognition with experience-dependent learning, Neural Comput. 5 (2010) 1333–1357.

[36] Oleynik A, Ponosov A and Wyller J On the properties of nonlinear nonlocal operators arising in neural field models, Accepted for publication in Journal of Mathematical Analysis and Applications, 2012.

[37] Yousaf M, Ponosov A, Wyller J, Einevoll GT Neural firing rate model with a steep firing rate function, Nonlinear Analysis: Real World App., doi:10.1016/j.nonrwa.2012.07.031. In press, 2012.